Journal of Adhesion Science and Technology

ISSN: 0169-4243 (Print) 1568-5616 (Online) Journal homepage: https://www.tandfonline.com/loi/tast20

A holistic mathematical modelling and simulation for cathodic delamination mechanism – a novel and an efficient approach

M.H. Nazir, Z.A. Khan & K. Stokes

To cite this article: M.H. Nazir, Z.A. Khan & K. Stokes (2015) A holistic mathematical modelling and simulation for cathodic delamination mechanism – a novel and an efficient approach, Journal of Adhesion Science and Technology, 29:22, 2475-2513, DOI: 10.1080/01694243.2015.1071023

To link to this article: https://doi.org/10.1080/01694243.2015.1071023

Published online: 11 Aug 2015.

Journal of Adhesion Science and Technology, 2015
Vol. 29, No. 22, 2475–2513, http://dx.doi.org/10.1080/01694243.2015.1071023

Taylor & Francis
Taylor & Francis Group

A holistic mathematical modelling and simulation for cathodic delamination mechanism – a novel and an efficient approach

M.H. Nazir[a]*, Z.A. Khan[a] and K. Stokes[b]

[a]*Bournemouth University, Sustainable Design Research Centre (SDRC), Poole BH12 5BB, UK;*
[b]*Defence Science and Technology Laboratory (DSTL), Salisbury, UK*

(*Received 31 March 2015; accepted 5 July 2015*)

This paper addresses a holistic mathematical design using a novel approach for understanding the mechanism of cathodic delamination. The approach employed a set of interdependent parallel processes with each process representing: cation formation, oxygen reduction and cation transport mechanism, respectively. Novel mathematical equations have been developed for each of the processes based on the observations recorded from experimentation. These equations are then solved using efficient time-iterated algorithms. Each process consists of distinct algorithms which communicate with each other using duplex channels carrying signals. Each signal represents a distinct delamination parameter. As a result of interdependency of various processes and their parallel behaviour, it is much easier to analyse the quantitative agreement between various delamination parameters. The developed modelling approach provides an efficient and reliable prediction method for the delamination failure. The results obtained are in good agreement with the previously reported experimental interpretations and numerical results. This model provides a foundation for the future research within the area of coating failure analysis and prediction.

Keywords: paint; coating; delamination; blister; coating failure; diffusion; corrosion; mathematical modelling; simulations; partial differential equations; iterative algorithm

Nomenclature

c_s	Ionic concentration along the metal-coating interface
Φ	Electrolyte potential
x_p	Position of peak potential plot
t	Time passed after the defect encounters solution electrolyte
t_n	Minimum time required to actuate the defect
η	Slope of the plot
x	Distance to the defect along the interface
$\bar{x}$	Mean diffusion length for the effective ionic species
c_{S_o}	Concentration of cations along the metal-coating interface adjacent to the defect
D_{A_S}	Mean of standard diffusion coefficient of all the ionic species
$D_{S,STA_{ion}}$	Standard diffusion coefficient of ionic species
T	Temperature
RH	Pore relative humidity

*Corresponding author: Email: hnazir@bournemouth.ac.uk

t_{exp}	Time of exposure
G	Activation energy
T_{STA}	Standard absolute temperature
RH_{STA}	Standard relative humidity at which D_{A_S} drops between maximum and minimum
m	Parameter that characterises the spread of drop at RH_{STA}
t_{STA}	Time of exposure at which D_{A_S} is measured (normally 1 month)
t_a	Actual time of exposure
n_{ag}	Age reduction factor
$c_{S_{TH}}$	Cation threshold concentration
c_{S_B}	Bulk electrolyte (ionic) concentration
$c_{S_B}^{TH}$	Minimum concentration of the bulk electrolyte required to start the process of delamination
$kc_{S_{eq}}$	Parameter defining ratio of c_{S_o} to c_{S_B}
i_{Fe}^{aq}	Exchange current density
E_{Fe}^{o}	Equilibrium potential
β_{Fe}	Iron Tafel slope
$i_{i_o,Fe}^{coat}$	Current density as a result of iron dissolution at the 'iron – coating' interface
$i_{o,Fe}$	current density due to the iron dissolution forward reaction for the bare iron in an aqueous medium
$w_{Fe} = i_{o,Fe}^{coat}/i_{o,Fe}$	Parameter representing the difference in effect between 'iron – coating' interface and the 'electrolyte – iron' interface
w_{O_2}	Parameter representing the reduction in mass transfer due to the presence of ionic salt film within porous medium
w_e	Parameter defining the ratio of surface available for the electrochemical reaction per total surface area
i_{lim,O_2}^{coat}	Mass transfer limited current density
g_m	Thickness of degraded coating
g_c	Thickness of non-degraded coating
ε_c	Porosity for non-degraded coating
ε_m	Porosity for degraded coating
$b_{w_{O_{2,1}}} - b_{w_{O_{2,7}}}$	Fitting parameters for non-linear function of w_{O_2}–pH relationship
$b_{w_{Fe_1}} - b_{w_{Fe_4}}$	Fitting parameters for non-linear function of w_{Fe}–pH relationship
$\partial c_s/\partial t$	Time-dependent ionic concentration along the interface
kn_{eq}	Parameter defining ratio of production of OH^- after the electrochemical reaction along the interface to the concentration of oxygen
N_s	Diffusion flux
R_s	Rate of homogeneous reaction
J_m	Mass flux

Abbreviations

SDL	System and description language
CDB	Cathodic delamination block
CTM	Cation transport modelling
IPM	Interfacial propagation modelling
DCM	Delaminated coating modelling

1. Introduction

Cathodic delamination is one of the most vital processes responsible for the metal-coating degradation.[1] Continuous on-going electrochemical reactions beneath the metal-coating results in the delamination of coating. Atmospheric pollutants are present in bulk amount at the metal-coating defect. These atmospheric pollutants are the source for many ionic species that contribute towards the alkalinisation of electrolyte solution. The ionic species are continuously transported by the bulk solution into the delaminated region, resulting in the formation of an electrochemical cell. Metal is oxidised at the anodic sites, while oxygen is reduced at the cathodic sites.[2] The cathodic-induced sites act as 'nucleation sites for cathodic delamination'. The transport of these ionic species from a defect into the delaminated region is considered to be the rate-determining step for cathodic delamination. Along with the transport of ionic species through the defect, the transport of oxygen and water through the coating is also important for the progression of delamination process, but normally these two parameters are sufficiently available. The reduction of oxygen results in the pH change of the electrolyte solution due to the production of OH^- anions. Although initially anions and cations largely incorporate into the delamination region, overall cations are in excess when compared to anions.[3] Normally a linear progression of delamination with respect to time is witnessed. This linear behaviour can be explained by the alkalisation effect on the electrolyte solution due to oxygen reduction.

Ogle [4] developed the relationships for the rate of metal-coating delamination and the anodic/cathodic current density using a special electrochemical cell and provided with the solution to decelerate the delamination rate by evacuating the defected coating from alkaline electrolyte species.[5,6] Stratmann and Leng [7–15] investigated the cathodic delamination process in the defected area using various experimental techniques. The experimental findings by Startmann indicated that the driving factor for the metal-coating delamination is the diffusion of ions from the defected site to the interface. His further findings showed that the corrosion rate decreases with the large concentration of ionic species diffusing through the defect resulting in the passivation and making the active metal sites to appear beneath the metal-coating. Allahar [16] developed a mathematical model based upon the experimental results of Stratmann and further extended his research work and designed a non-linear porosity–pH relationship. Based upon Allahar's approach, Huang [17] investigated that the OH^- ions along the metal-coating interface decide the propagation of metal-coating delamination; his further investigation showed that the delamination rate depends upon the metal-coating bond breakage. When the time constant associated with the metal-coating bond breakage is small, the migration and the diffusion rate of ionic species into the delaminated region is also small.[17]

However, Allahar [16], Huang [17], Stratmann [3,7] and Leng [9,11] investigations did not cover the effect of environmental parameters such as: temperature variations (T), time of exposure (t_{exp}) and pore relative humidity (RH). Allahar modelled the polarisation kinetics, influenced by just oxygen reduction reaction without the influence of environmental parameters (T, RH and t_{exp}). Similarly, Stratmann's [3,7] and Leng's [9,11] experimental approach covered the effect of cation transport on the delamination process but did not consider the effect of environmental parameters. Also neither of the conventional methods modelled a complete cathodic delamination system using an efficient time iterative approach. The developed iterative approach in this paper produced much more efficient results compared to the numerical approach used by Allahar [16] and Huang [17].

All these environmental parameters (T, RH and t_{exp}) and an efficient design methodology have been taken into an account in the developed model. This work is

the continuation of research within our group.[2,18–26] A mathematical model is developed which is then solved using a system and description language [27,28] with well-defined interdependent processes. All the processes are modelled as flowchart algorithms which can be further used to create FSM (finite state machines) or writing a programme. The developed model couples and simulates the effect of cations formation, oxygen reduction and cations transport using parallel processes approach. Each process models the following mechanisms of delamination, respectively:

(1) Alkaline hydrolysis of the coating (Cation formation).
(2) Oxygen reduction.
(3) Cation transport along the interface of metal-coating.

Previous studies on cathodic delamination were focused on experimental research. However, there was always a need for an efficient mathematical model along with a time-iterated system that can solve a system of PDE's (partial differential equations) for delamination process with optimum accuracy. The time-iterated system in this paper consists of interdependent processes with each process having a distinct algorithm. These process algorithms communicate with each other using channels with specific signal lists. These signal lists comprise all parameters which influence the metal-coating delamination. At the end, the model is utilised to find the remaining useful life (RUL) of a metal-coating system based on the probability of failure of metal-coating bonding.

The model is based on the observations recorded from experimentation. These experiments are performed to understand the behaviour of metal-coating delamination under the effect of various salt solutions.

2. Experimental set-up and observations

2.1. Sample preparation

AISI 1010 carbon steel is used as a substrate and primer (red-oxide) is used as a coating in this paper. The primer is sprayed using a conventional spraying gun. The experiment is designed to analyse the effect of NaCl and KCl solutions with various molar concentrations i.e. 0.01, 0.5 and 1 M. 500 ml of de-ionised water is used to prepare NaCl and KCl solutions. Six samples were prepared with the same coating thickness (23 μm) and the same interface roughness (5.3 μm). The values of coating thickness and interface roughness are measured using 3-D scanning interferometry.[29] These thickness and roughness values are averaged through 10 data points per sample. All the samples were coated at the same time with the same coating type and under the same conditions.

2.2. Experimental observations

Samples 1, 2 and 3 were exposed to NaCl solution with 0.01, 0.5 and 1 M solution concentrations, respectively. However, samples 4, 5 and 6 were exposed to KCl solution with 0.01, 0.5 and 1 M solution concentrations, respectively, as shown in Table 1. The exposure test was performed to investigate the delamination of coated samples under the effect of NaCl and KCl solutions. This exposure of samples to NaCl and KCl solutions resulted in the delamination of coatings due to the diffusing salts through microscopic defects on coatings. The samples were then removed from the salt solutions and the cross-sectional analysis of each sample was performed under the microscope. The evaluation of delaminated regions was performed using scanning electron microscope (SEM). The SEM was used for the measurement of 'coating uplift' (or

Table 1. Experimental observations: cross-sectional images of coated samples exposed to NaCl and KCl solution with various molar concentrations: 0.01, 0.5 and 1 M.

Molar concentration	NaCl	KCl
0.01 M	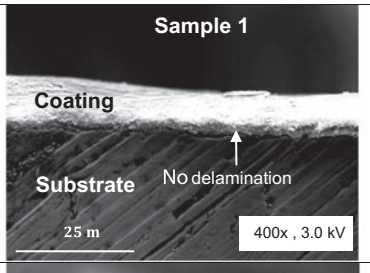	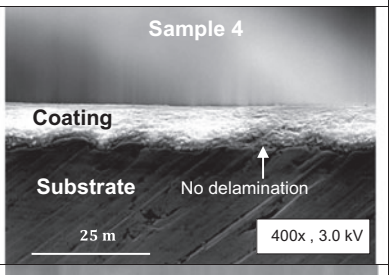
0.5 M	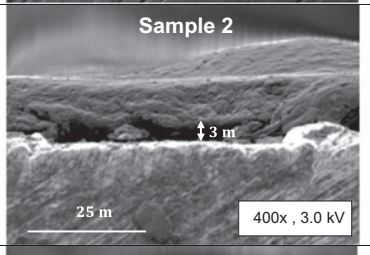	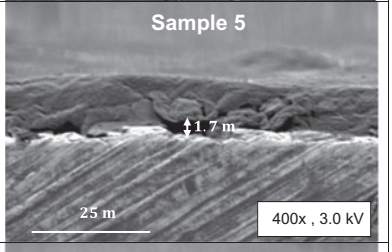
1 M	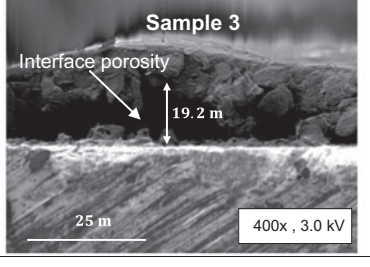	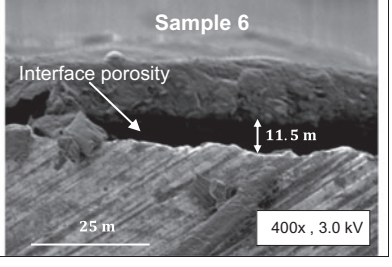

interface porosity) as a result of delamination as shown in Table 1. Following observations were made from the post exposure analysis of the samples.

(1) The samples (3 and 6) which were exposed to (high pH) high molar concentration (1 M) of NaCl and KCl, respectively, exhibit a higher uplift of coating (or interface porosity) due to the delamination. The samples (2 and 5) which were exposed to a (low pH) low molar concentration (0.5 M) exhibit smaller uplift of coating (or interface porosity) due to the delamination. The samples (1 and 4) which were exposed to 0.01 M exhibit no uplift of coating (or interface porosity).
(2) The experiment clearly indicates that for the coating to exhibit uplift (or interface porosity), the molar concentration of salts must be greater than some threshold concentration. In this experiment, the coating did not show the uplift for molar concentration 0.01 M, therefore, 0.01 M concentration is thought to be less than the threshold concentration.
(3) The samples (1, 2 and 3) which were exposed to NaCl solutions showed higher uplift of coating compared to the samples (4, 5 and 6) which were exposed to KCl solutions. This is due to the size of hydrated cations, as potassium cation (K^+) is larger compared to sodium cation (Na^+). Larger sized hydrated cations have smaller delamination kinetics in aqueous medium [3], therefore, the delamination rate of samples exposed to KCl solutions is less than the samples exposed to NaCl solutions.

(4) SEM analysis of the samples showed that the 'coating uplift' (or interface porosity) was found right beside the microscopic defects on coatings as shown in Table 1. The microscopic defects were the incubation points for the 'coating uplift'. The defects allowed the cations to transport between anodic and cathodic corrosion sites at the interface. These sites resulted in the 'coating uplift' (or interface porosity) and ultimately leading to cathodic delamination. Dissolved oxygen along with solution, upon reduction produced OH^- and accelerated the cathodic delamination. Inside the delaminated (porous) region, Na^+ and K^+ acts as cation, while OH^- ions act as majority anions.

$$O_2 + 2H_2O + 4e^- \rightarrow OH^-$$

- Na^+ and K^+ were negligible in case of samples 1 and 4 (0.01 M) hence, no delamination was found despite the fact that samples had considerable microscopic defects on the coating. However, due to the negligible alkaline ionic species (Na^+ and K^+), the defects did not result in the delamination of coating.

Next, sections explain the development of a mathematical model based on the observations made from experimentation.

3. Mathematical model for metal-coating delamination mechanism

A schematic representation of a metal-coating delamination system along with water soluble salts and oxygen ingress through defect and pores in coating is shown in Figure 1. Depending upon the transport of these external agents through the failed protective coating, the area for metal-coating interface can be divided in three regions i.e. delaminated (porous), front and intact. Both the type and concentration of cations have a remarkable effect on the delamination rate which is already discussed in Section 2. Below the threshold concentration of cations at the defect, the process of delamination impedes.[3] The minimum threshold concentration of cations is necessary at the metal-coating defect in order to establish the required rate of oxygen reduction

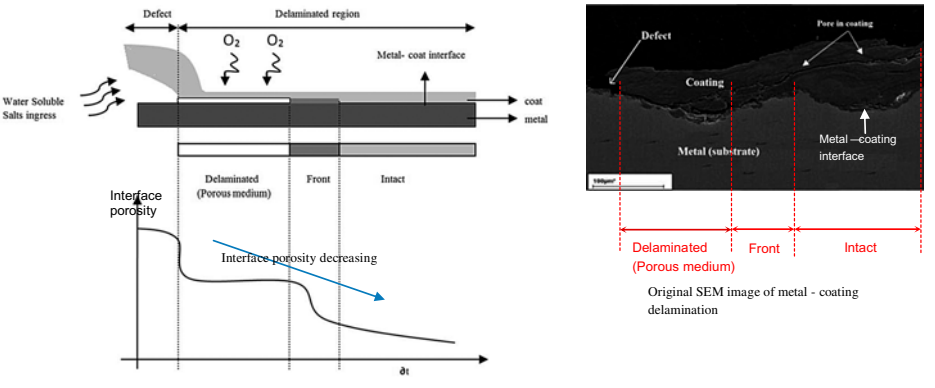

Figure 1. Schematic representation (on left) of metal-coating delamination based on the original SEM image (on right). The metal is exposed to atmosphere through delaminated zone because of coating defect which provides an inlet to external environmental pollutants. Figure has been taken from our research paper [19].

as a result of electrochemical reaction. Thus, the delamination rate depends upon the dilution factor [30] of the electrolyte solution along the metal-coating interface. If the dilution factor is greater than there are not enough cations that can incorporate. In such situation, the extended diffuse double layer [31] dominates at the interface which in turn blocks the electrochemical reactions.

The electrolyte solution is assumed to follow the electro neutrality condition i.e. the rate of transport of cations from the defect must be equal to the rate of production of OH^- ions due to oxygen reduction reaction inside the delaminated (porous) region or front region. Therefore, the rate of production of OH^- ions (or pH) is decided by the rate of transport of cations. The interfacial propagation of delaminated (porous) region into the front end is dependent upon the local pH of an electrolyte solution (i.e. pH from 10 to 14).

It is assumed that the bulk conditions exist for ionic concentration (c_s) and electrolyte potential (Φ) at the opening of the defected portion. These bulk quantities are denoted as c_{S_B} and Φ_B. The electrolyte potential Φ is assumed to follow electro neutrality condition at all the boundaries as,

$$\Phi = \sum_{s=1}^{y} z_s c_s = 0$$

z_s defines the charge no. of species with concentration c_s, where $s = 1, 2 \ldots y$ represents the number of ionic species involved.

The metal-coating delamination mechanism can be represented in the form of a block which is termed as cathodic delamination block (CDB). CDB encapsulates three parallel processes which are interconnected using duplex channels as shown in Figure 2. These processes are termed as: delaminated coating modelling (DCM), cation transport modelling (CTM) and interfacial propagation modelling (IPM). All the processes inside the block CDB follow the electro neutrality condition.

Next, sections discuss the development of governing equations for each of the processes i.e. CTM, IPM and DCM, respectively.

3.1. *Cation transport modelling*

CTM models the diffusion of cations through the defect into delaminated (porous) region. The delamination rate depends upon diffusion of cations which decides the concentration of cations along the metal-coating interface. A well-known solution of the differential equation for Fick's second law can be utilised to model the change in ionic concentration due to the change in diffusion with time as,

$$c_s = c_{S_B}\left[1 - erf\left(\frac{x}{\bar{x}}\right)\right]; \quad c_s = c_{S_B} \text{when} \begin{cases} x = 0 \\ t = 0 \end{cases} \tag{1}$$

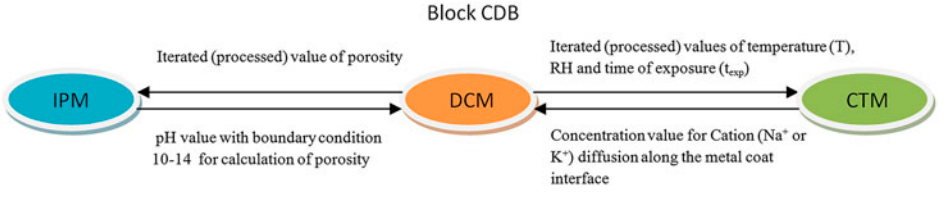

Figure 2. Modelling methodology, showing duplex communication between processes 'DCM-IPM' and 'DCM-CTM'.

Equation (1) shows the boundary conditions for ionic concentration c_s along the interface. Where x is the distance to the defect, c_{S_B} is the bulk concentration of electrolyte at the metal-coating defect. $\bar{x}$ is the mean diffusion length corresponding to the effective ionic diffusion time t. Where $\bar{x}$ is given as,[3]

$$\bar{x} = 2\sqrt{D_{A_S} t}$$

D_{A_S} is the average of standard diffusion coefficient of all the ionic species. This can be written as,

$$D_{A_S}\left(T, \mathrm{RH}, t_{\exp}\right) = \left[D_{S,\mathrm{STA}_{\mathrm{ion}}} F_1(T) F_2(\mathrm{RH}) F_3\left(t_{\exp}\right)\right]^{-2} \tag{2}$$

The diffusion coefficient $D_{S,\mathrm{STA}_{\mathrm{ion}}}$ of each ionic species along the metal-coating interface depends upon the temperature (T), pore relative humidity (RH) and time of exposure ($t_{\exp}$). The diffusion coefficient $D_{S,\mathrm{STA}_{\mathrm{ion}}}$ of the ionic species along the interface is two order smaller than in aqueous solution [7] as shown in Table 2.

3.1.1. $F_1(T)$: the temperature variation function in Equation (2) is given as [32]

$$F_1(T) = \exp\left[\left(\frac{G_a}{R}\right)\left(\frac{1}{T_{\mathrm{STA}}} - \frac{1}{T}\right)\right] \tag{3}$$

Equation (3) represents the situation for temperature variation from T_{STA} to T, G_a is the activation energy of ionic species during the diffusion process, R is the Universal gas constant and T_{STA} is the standard temperature value.

3.1.2. $F_2(\mathrm{RH})$: the relative humidity variation function is given as: [7]

$$F_2(\mathrm{RH}) = \frac{1}{1 + \left(\frac{1-\mathrm{RH}}{1-\mathrm{RH}_{\mathrm{STA}}}\right)^{\mathrm{m}}} \tag{4}$$

where RH is the actual pore relative humidity, $\mathrm{RH}_{\mathrm{STA}}$ is the standard relative humidity at which D_{A_S} drops between maximum and minimum values and m is the parameter that characterises the spread of drop in $\mathrm{RH}_{\mathrm{STA}}$.[17]

3.1.3. F_3 (t_{exp}) the ageing function which takes into account the time of exposure is given as

$$F_3\left(t_{\exp}\right) = \left(\frac{t_{\mathrm{STA}}}{t_a}\right)^{\mathrm{n_{ag}}} \tag{5}$$

Table 2. Diffusion coefficient values for ionic species in aqueous solution and metal-coating interface inside delaminated porous region [cm^2/s].

Ionic species	D in Bulk aqueous solution (bulk electrolyte)	$D_{S,\mathrm{STAion}}$ at metal-coating interface
K^+	1.84×10^{-5}	8.4×10^{-7}
Na^+	1.47×10^{-5}	6.4×10^{-7}
Fe^{2+}	0.719×10^{-5}	0.5×10^{-7}
OH^-	0.527×10^{-5}	6.1×10^{-7}

where t_{STA} is the time of exposure at which D_{As} is measured (normally 1 month), t_a is the actual time of exposure and n_{ag} is the age reduction factor.

The threshold concentration of cations, c_S^{TH} which is required to be achieved in order to start the process of delamination by galvanically coupling the intact region to the defect is given as,

$$c_S^{TH} = c_{S_o}\left[1 - erf\left(\frac{x_p}{\bar{x}}\right)\right] = kc_{s_{eq}} \cdot c_{S_B}\left[1 - erf\left(\frac{x_p}{\bar{x}}\right)\right] \tag{6}$$

The term x_p is the position of peak potential along the metal-coating interface as shown in Figure 3. Certain potential change between delaminated (porous) point along the interface and intact region imitates the presence of diatomic OH^- ions. The peak potential defines the position of electrochemical reaction along the metal-coating interface with respect to time and is given as,[10]

$$x_p = \eta\sqrt{t_p}; \quad t_p = t - t_n \tag{7}$$

where η represents the mobility constant of cations, t is the time passed after the defect encounters the solution electrolyte, t_n is the minimum time required to actuate the defect (or incubation time). The term c_{S_o} in Equation (6) is the concentration of cations along the metal-coating interface adjacent to the defect. The concentration c_{S_o} may be equal to the bulk concentration of electrolyte c_{S_B} at the defect such that, $c_{S_o} = c_{S_B}$. However, c_{S_o} can also represent the equilibrium concentration of ions at the interface in contact with the bulk electrolyte. In this research, a simple equation for the equilibrium constant $kc_{s_{eq}}$ is used such that, $kc_{s_{eq}} = (c_{S_o}\ c_{S_B})$.

Equation (6) can be rewritten in order to find the minimum concentration of the bulk electrolyte $c_{S_B}^{TH}$ to start the process of delamination.

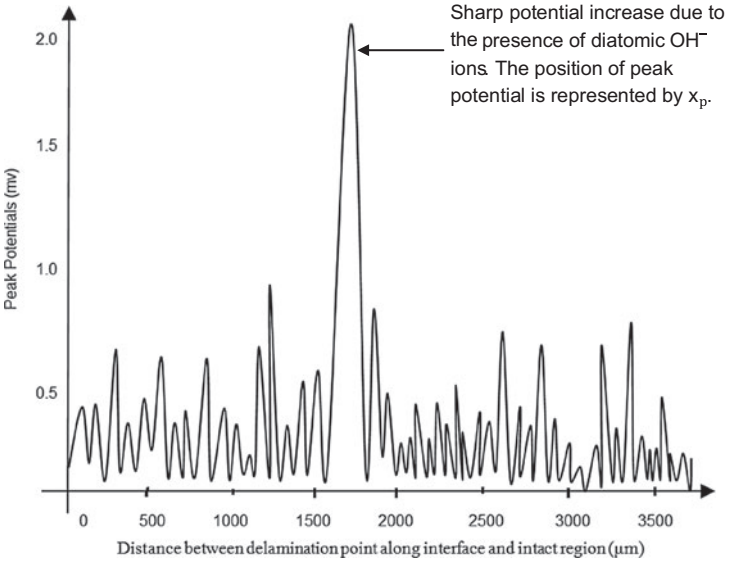

Figure 3. Potential gradient profile along metal-coating interface [2].

$$c_{S_B}^{TH} = \frac{c_S^{TH}}{k c_{S_{eq}}} = c_{S_B}\left[1 - erf\left(\frac{x_p}{\bar{x}}\right)\right] \tag{8}$$

3.2. *Interfacial propagation modelling*

IPM models the propagation of front end along the metal-coating interface as a result of iron oxidation and oxygen reduction. The propagation of front end along the interface depends upon the pH-polarisation kinetics relationships for iron and oxygen. Keeping electro neutrality condition, it is assumed that pH is dependent upon the concentration of cations along the metal-coating interface. Thus, higher concentration of cations means higher pH which in turn affects the polarisation parameters (w_{Fe}, w_{O_2} and interface porosity (ε). These two (polarisation parameters and interface porosity) in turn affect the polarisation kinetics for iron dissolution and oxygen reduction. Local pH of electrolyte solution is assumed to vary from 10 to 14 depending upon the varying ionic concentration. IPM considers Fe^{2+}, Na^+ and OH^- as active ionic species during the delamination process. No homogeneous reactions are taken into account; just electrochemical reactions are considered which include iron dissolution and oxygen reduction reactions. Iron dissolution and oxygen reduction are the two main electrochemical reactions of interest in the current research. The expressions of the polarisation kinetics for iron dissolution and oxygen reduction are developed.

3.2.1. *Iron dissolution (polarisation kinetics)*

The polarisation kinetics for the forward reaction involving iron dissolution is expressed as,

$$Fe \rightarrow Fe^{2+} + 2e^-$$

In this research, only forward reaction is considered because backward reaction involves iron deposition which can be neglected.[16] The current density i_{Fe}^{aq} due to the 'iron dissolution forward reaction' for the bare iron in an aqueous medium is given as, [17]

$$i_{Fe}^{aq} = i_{o,Fe} 10^{\frac{V - E_{Fe}^o}{\beta_{Fe}}}; \quad V = E - \Phi \tag{9}$$

where $i_{o,Fe}$, E_{Fe}^o, E and β_{Fe} are the exchange current density, equilibrium potential, metal potential and iron–Tafel slope, respectively. Equation (9) can be modified to derive the current density i_{Fe}^{coat} at the 'iron–coating' interface as a result of iron dissolution as,

$$i_{Fe}^{coat} = w_e w_{Fe} i_{o,Fe} 10^{\frac{V - E_{Fe}^o}{\beta_{Fe}}} \tag{10}$$

where w_e is the surface area of the electrochemical reaction and is defined as the ratio of surface available for the electrochemical reaction per total surface area. At 'iron–coating' interface, the exchange current density would be different from the 'iron–electrolyte' interface.[16] This difference in effect is considered using polarisation parameter w_{Fe} where $w_{Fe} = \frac{i_{o,Fe}^{coat}}{i_{o,Fe}}$.

3.2.2. Oxygen reduction (polarisation kinetics)

The polarisation kinetics for the reaction involving oxygen reduction is expressed as,

$$O_2 + 2H_2O + 4e^- \rightarrow 4OH^-$$

The current density due to the oxygen reduction along the metal-coating interface is given as,[16]

$$i_{O_2}^{coat} = -w_e w_{O_2} i_{lim,O_2}^{coat} \tag{11}$$

where polarisation parameter w_{O_2} refers to the reduction in mass transfer due to the presence of ionic salt film along the interface, i_{lim,O_2}^{coat} refers to the mass transfer limited current density and is given as,

$$i_{lim,O_2}^{coat} = -nFD_{O_2}c_{O_2}\left(\frac{\varepsilon_m^{1.5}\varepsilon_c^{1.5}}{\varepsilon_m^{1.5}g_c + \varepsilon_c^{1.5}g_m}\right) \tag{12}$$

where g_m and g_c are the thickness of the degraded and non-degraded coating, respectively, and ε_m and ε_c are the interface porosities for degraded and non-degraded coating, respectively. The term c_{O_2} represents the dissolved concentration of oxygen at coating surface, D_{O_2} is the diffusion coefficients for oxygen, F is the Faradays constant and n is the number of electrons transferred.[33]

3.2.3. Polarisation parameters (w_{Fe}, w_{O_2})–pH relationship

The polarisation parameters w_{Fe} and w_{O_2} in Equations (10) and (11), respectively, are the functions of pH. Separate expressions for the both the polarisation parameters have been developed. These expressions are based on non-linear sigmoid functions as shown in Figure 4(a) and (b). The shape for the trends of non-linear sigmoid functions is based on the observations made from experimentation in Section 2.

The variable profile for w_{O_2} in various regions is assumed to be the function of pH. The formulation for w_{O_2}–pH is obtained using the fitting parameters ($b_{w_{O_{2,1}}} - b_{w_{O_{2,7}}}$) for non-linear function as,

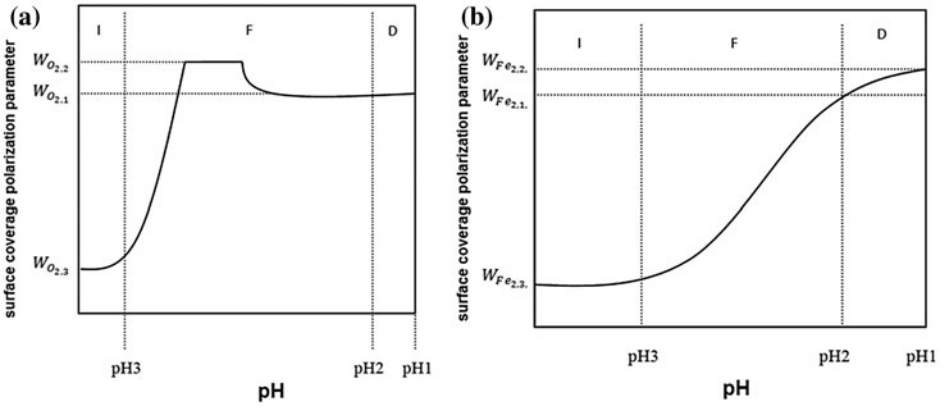

Figure 4. Polarisation kinetics parameter curves for (a) O_2 and (b) Fe^{2+} w.r.t pH using curve fitting values from Table 3.

$$w_{O_2}(\mathrm{pH}) = \frac{b_{w_{O_{2,1}}} \exp\left[-b_{w_{O_{2,2}}}\left(pH - b_{w_{O_{2,3}}}\right)\right]}{1 + b_{w_{O_{2,4}}} \exp\left[-b_{w_{O_{2,5}}}\left(pH - b_{w_{O_{2,6}}}\right)\right]} + b_{w_{O_{2,7}}} \tag{13}$$

The parameter w_{Fe} is used to account for the nature of interface on iron dissolution reaction. The w_{Fe}–pH relationship is formulated using fitting parameters ($b_{w_{Fe_1}} - b_{w_{Fe_4}}$) for non-linear function as,

$$w_{Fe}(\mathrm{pH}) = \frac{b_{w_{Fe_1}}}{1 + \exp\left[b_{w_{Fe_2}}\left(\mathrm{pH} - b_{w_{Fe,3}}\right)\right]} + b_{w_{Fe_4}} \tag{14}$$

The curve fitting values of w_{Fe} and w_{O_2}, which are used during this research, are shown in Table 3. The notations 'I', 'F' and 'D' in the graphs in Figure 4(a) and (b) indicate the intact, front and delaminated regions, respectively, along the interface.

3.2.4. *Interface porosity (ε)–pH relationship*

The interface porosity ε in Equation (12) is a function of pH. Experimental observations in Section 2 showed that at high pH, bonding strength is low while at low pH, bonding strength is high. This supports the assumption that OH^- ions play a vital role in the degradation by weakening the metal-coating bonding strength. Similarly, high interface porosity ε accounts for low bonding strength while low interface porosity ε accounts for high bonding strength (Figure 5).

Based on the experimental observations, the formulation for ε–pH is developed by fitting an equation of the form as,

$$\varepsilon(\mathrm{pH}) = \frac{b_{\varepsilon,1}}{1 + \exp\left[b_{\varepsilon,2}\left(pH - b_{\varepsilon,3}\right)\right]} + b_{\varepsilon,4} \tag{15}$$

where $b_{\varepsilon,1}$–$b_{\varepsilon,4}$ are the fitting parameters. Equation (15) governs the equilibrium relationship under the assumption that the time constant associated with the bond breakage and degradation is sufficiently small such that an equilibrium value of ε is attained instantaneously with the change in pH.

On the other hand when the time constant for the bond breakage and degradation is large compared to the time constant for diffusion and migration, the value of ε attained instantaneously is not valid. A non-equilibrium relationship between ε and pH is,

$$\frac{\partial \varepsilon}{\partial t} = kn_{eq}\left(\varepsilon_{eq} - \varepsilon\right) \tag{16}$$

Table 3. Curve fitting values for polarisation parameters w_{Fe} and w_{Fe}.

b_i	w_{O_2}	w_{Fe}
1	−30	4.5
2	9.5	4.8
3	9.8	10.4
4	−20	10.9
5	−0.5	–
6	−40	–
7	−11	–

Table 4. Curve fitting values for polarisation parameters porosity–pH sigmoid curve.

b_i	ε
1	0.3
2	0.1
3	4.3
4	5×10^{-3}

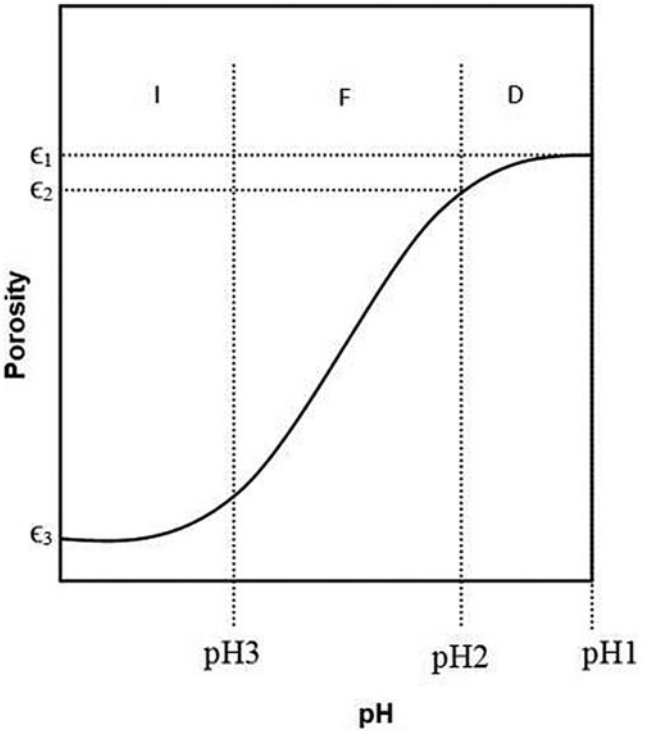

Figure 5. Porosity-pH sigmoid curve using fitting parameters from Table 4.

where ε_{eq} is obtained from Equation (15) and kn_{eq} is the rate reaction for the bond breakage resulting in OH^- production, same as $kc_{s_{eq}}$ which is discussed in Equation (6). Therefore, $kn_{eq} = \frac{[P]_{eq}}{[R]_{eq}}$, where P represents the production of OH^- after the electrochemical reaction along the interface while R represents the concentration of oxygen. If $kn_{eq} > 0$ than ε attains equilibrium value $(\varepsilon - \varepsilon_{eq})$ while for $kn_{eq} = 0$ than $\frac{\partial \varepsilon}{\partial t} \approx 0$ and porosity remains constant.

3.3. *Delaminated coating modelling*

DCM models the time-dependent values of ionic concentration along the metal-coating interface. The timely variation of ionic concentration along the interface depends upon temperature (T), pore relative humidity (RH), time of exposure (t_{exp}) and ε. DCM makes use of the inputs coming from CTM and IPM, respectively, and simulates the

time-dependent ionic concentration $\frac{\partial c_s}{\partial t}$ for electrochemically active species (Fe^{2+}, Na^+ and OH^-) along the metal-coating interface. DCM takes temperature (T), pore relative humidity (RH), time of exposure (t_{exp}) as input parameters from CTM and ε as an input parameter from IPM, respectively. The ionic concentration $\frac{\partial c_s}{\partial t}$ is the final output and is used to analyse the rate of delamination along the metal-coating interface. Also, DCM processes (iterates with respect to time) the input parameters (T, RH, t_{exp},) ε and again returns the processed values ($T_i, RH_i, t_{exp,i}, \varepsilon_i$) to CTM and IPM, respectively.

Fick's second law of diffusion in conjunction with the law of conservation of mass can be used to find the ionic concentration $\frac{\partial c_s}{\partial t}$ (electro-diffusion) in an electrochemical system as,[34,35]

$$\frac{\partial c_s}{\partial t} = -\nabla \cdot N_s + R_s + S_s \tag{17}$$

where N_s represents the flux of ionic species, R_s represents the rate of homogeneous reaction and S_s represents the production of ions per unit volume by electrochemical reactions. The flux of ionic species (Fe^{2+}, Na^+ and OH^-) at the delaminated (porous) region along the interface is given as,[36]

$$N_s = -\underbrace{z_s D_{A_s} c_s \nabla \Phi}_{\text{Migration}} - \underbrace{D_{A_s} \nabla c_s}_{\text{Diffusion}} + \underbrace{c_s J_m}_{\text{Convection}} \tag{18}$$

where z_s represents the charge and J_m is the local electrolyte flux (velocity of the electrolyte). Equation (17) can be expanded by incorporating Equation (18), as,

$$\frac{\partial c_s}{\partial t} + c_s J_m = z_s D_{A_s} c_s \nabla \Phi + D_{A_s} \nabla c_s + R_s + S_s \tag{19}$$

Under the assumption that the electrolyte follows 'isochoric flow' ($J_m = 0$), convection part can be neglected. Therefore, conservation of mass yield's a governing equation for c_s in an electrolyte system. Equation (19) for electro-diffusion in an electrochemical system can be written as,

$$\frac{\partial c_s}{\partial t} = z_s D_{A_s} c_s \nabla \Phi + D_{A_s} \nabla c_s + R_s + S_s \tag{20}$$

The equation for the diffusion coefficient D_{A_s} (which is used in Equation (20)) has been previously derived in Equation (2). The diffusion coefficient equation D_{A_s} can now be combined with the porosity ε (which is used in Equation (15)) as,

$$D_{A_s}(T_i, RH_i, t_{exp,i}, \varepsilon_i) = \varepsilon^{1.5} \left[D_{S,STA_{ions}} F_1(T_i) F_2(RH_i) F_3(t_{exp,i}) \right]^{-2} \tag{21}$$

where $D_{S,STA_{ions}}$ is the standard diffusion coefficient for ionic species: Fe^{2+}, Na^+ and OH^- along the metal-coating interface as shown in Table 2. $T_i, RH_i, t_{exp,i}$ are the processed (iterated) inputs from DCM to CTM. The function values: $F_1(T_i), F_2(RH_i)$ and $F_3(t_{exp,i})$ in Equation (21) are calculated using Equations (3)–(5).

Equation (20) can be written in functional form by incorporating Equation (21) as,

$$\frac{\partial c_s}{\partial t}(T_i, RH_i, t_{exp,i}, \varepsilon_i) = z_s D_{A_s}(T_i, RH_i, t_{exp,i}, \varepsilon_i) c_s \nabla \Phi + D_{A_s}(T_i, RH_i, t_{exp,i}, \varepsilon_i) \nabla c_s + R_s + S_s \tag{22}$$

Equation (22) follows the law of conservation of mass, as the change in concentration of ionic species along the interface with time $\frac{\partial c_s}{\partial t}$ on the left side of Equation (22) must be equal to the sum of terms on the right side of equation. Equation (22) gives the relationship between ionic concentration along the interface $\frac{\partial c_s}{\partial t}$ with the interface porosity ε. The derived Equation (22) is consistent with the equation derived by Allahar [16] and Huang [17].

4. Mathematical model solution and implementation

4.1. System level design

The developed design consists of a model with the hierarchy as: system, block and processes. All these components are used in building a time-iterated model which involves parallel processing. The model for cathodic delamination along with hierarchies is shown in Figure 6.

The system level modelling consists of a top-most level of abstraction with the block termed as CDB. CDB consists of three parallel processes which are interconnected using channels ($r1$ to $r7$) with duplex communication. These processes are termed as: DCM, CTM and IPM. All the processes are modelled as flowchart algorithms which can be further used to create FSM or writing a programme. All these processes communicate with each other (using channels $r1$–$r7$) and with environment (using channels $c1$ and $c2$) as shown in Figure 6. The following sections discuss the method for solving each process using the governing equations for cathodic delamination mechanism.

4.2. Process CTM implementation (Proc. CTM)

(1) The algorithm for process CTM (Proc. CTM) is shown in Figure 7. The I/O channels with signal lists are shown in Table 5. Proc. CTM keeps a check on the threshold concentration of cations c_S^{TH} along the metal-coating interface.
(2) There are two input channels to the process i.e. $r1$ and r^2. The input channel $r1$ corresponds to the input from system (CDB) while input channel r^2 corresponds to the input from the process DCM (Proc. DCM). The input channel $r1$ from the system CDB corresponds to the signal list from the environment through

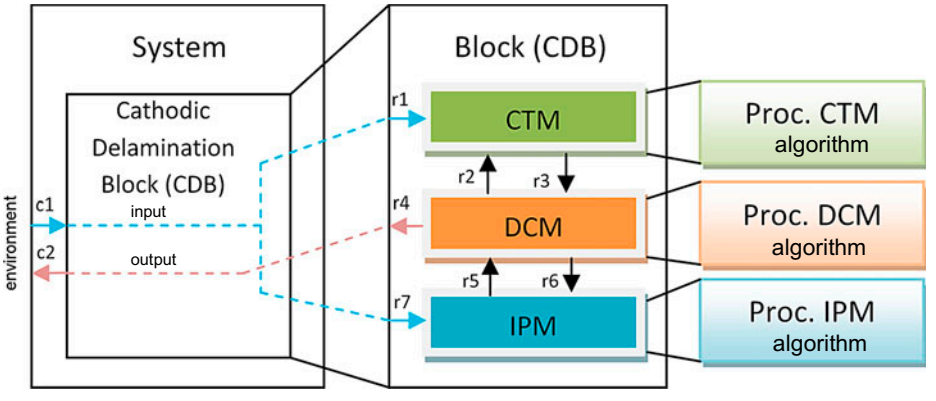

Figure 6. Structural view of cathodic delamination mechanism – a model.

channel $c1$. For input channel $r1$; sig T, sig RH, sig t_{exp} are the initial values at the start of simulation run and are assumed to remain constant till threshold condition is met. For input channel r^2 from process DCM; sig T_i, sig RH_i, sig $t_{exp,i}$ represent the time-dependent iterated (processed) values of T, RH and t_{exp}.

(3) Proc. CTM algorithm initiates with $c_S = c_{S_B}$ assuming the condition that concentration along the interface is equal to the bulk concentration at metal-coating

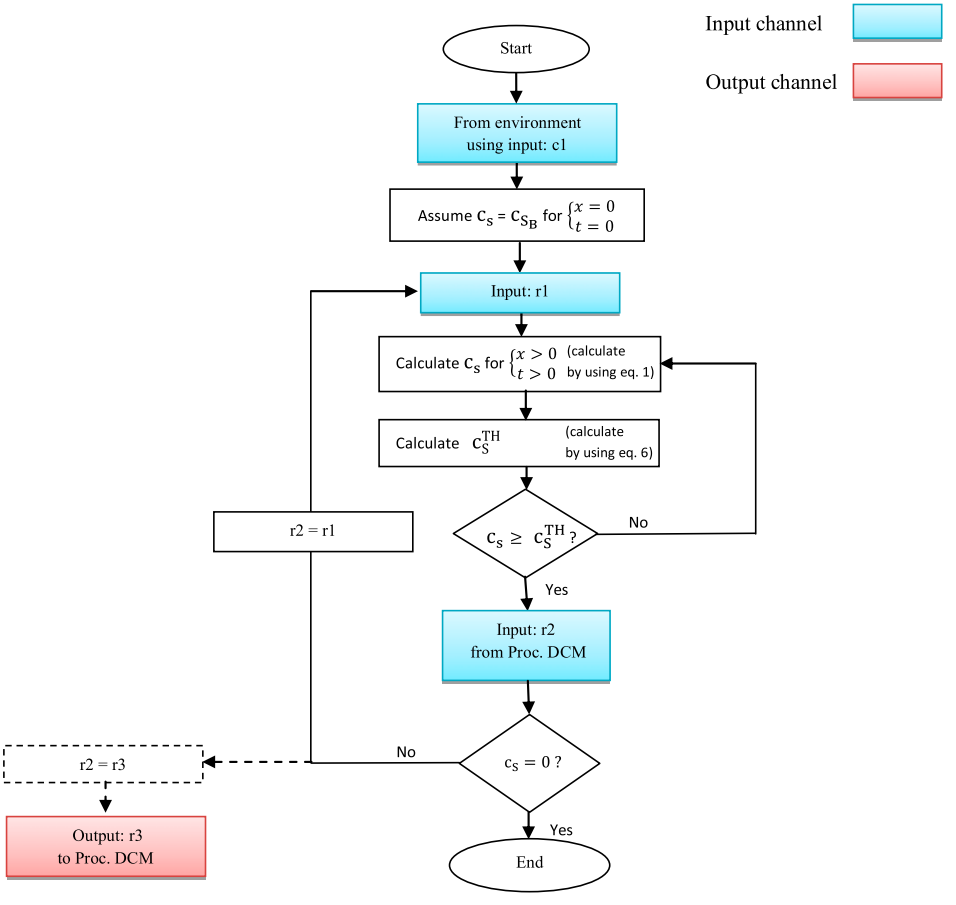

Figure 7. Algorithm for process CTM (Proc. CTM).

Table 5. I/O channels for Proc. CTM with their corresponding signal list.

Input channels		Output channel	
$c1$ $r1$ (from environment) r^2 (from Proc. DCM)	sig T, sig RH, sig t_{exp}, sig $D_{S,STA,cation}$, sig x, sig t, sig t, sig, sig t_n sig T_i, sig RH_i, sig $t_{exp,i}$	$r3$ (to Proc. DCM)	sig T, sig RH, sig t_{exp}

Note: Input channel ; Ouput channel .

defect. This condition is true if the distance to the defect is zero ($x = 0$) and the average ionic diffusion time is also zero ($t = 0$). Then process algorithm calculates the ionic concentration 'c_s' (using Equation (1)) along the interface and compares it with threshold concentration 'c_S^{TH}' required for delamination process initiation (where c_S^{TH} is calculated using Equation (6)). If the condition $c_s \geq c_S^{TH}$ is met, the algorithm starts taking the input from proc. DCM (will be discussed in the Section 4.4) through channel r^2.

(4) CTM simulates until condition $c_S = 0$ is met which means that the bulk concentration along the interface becomes zero. Upon condition if $c_S \neq 0$, it updates the current values (sig T, sig RH, sig t_{exp}) of input channel $r1$ after every iteration using $r^2 = r1$. Using the updated list of inputs, CTM calculates the current value of concentration along the metal-coating interface. However, if c_s becomes zero, it is assumed that the concentration of OH^- will automatically drop to maintain electro neutrality. This will result in pH drop (pH < 10) of electrolyte solution, in turn decreasing the metal-coating bond breakage and ceasing the delamination process.

(5) CTM also updates the current values of output channel $r3$ after each iteration using $r^2 = r3$. These output values from channel $r3$ are then fed as input values to Proc. DCM.

4.3. Process IPM implementation

(1) The algorithm for process IPM (Proc. IPM) is shown in Figure 8. The I/O channels with signal lists are shown in Table 6. Proc. IPM keeps a check on the change in pH value due to the electrochemical reactions along the metal-coating interface.

(2) Proc. IPM initiates by considering the inputs from channel $r7$. The input channel $r7$ from the system CDB corresponds to the signal list form the environment through channel $c1$.

(3) The input channel $r6$ from the Proc. DCM upgrades the values (pH) of channel $r7$ using $r6 = r7$. The iterated porosity ε_i value coming from Proc. DCM is used to calculate pH using modified form of Equation (15) as,

$$\mathrm{pH} = \frac{\log\left[\frac{b_{\varepsilon,1}}{\varepsilon - b_{\varepsilon,4}} - 1\right]}{b_{\varepsilon,2}} + b_{\varepsilon,3} \tag{23}$$

(4) Using calculated value of pH (using Equation (23)), Proc. IPM calculates the polarisation kinetics (using Equations (10) and (11)), polarisation parameters w_{Fe}, w_{O_2} (using Equations (13) and (14)) and interface porosity ε(using Equation (15)). The iterations of pH continue till the condition pH < 10 is met.

(5) Interface porosity (Equation (15)) is also retuned as an output (sig.) ε using channel $r5$. This output acts as an input value to Proc. DCM.

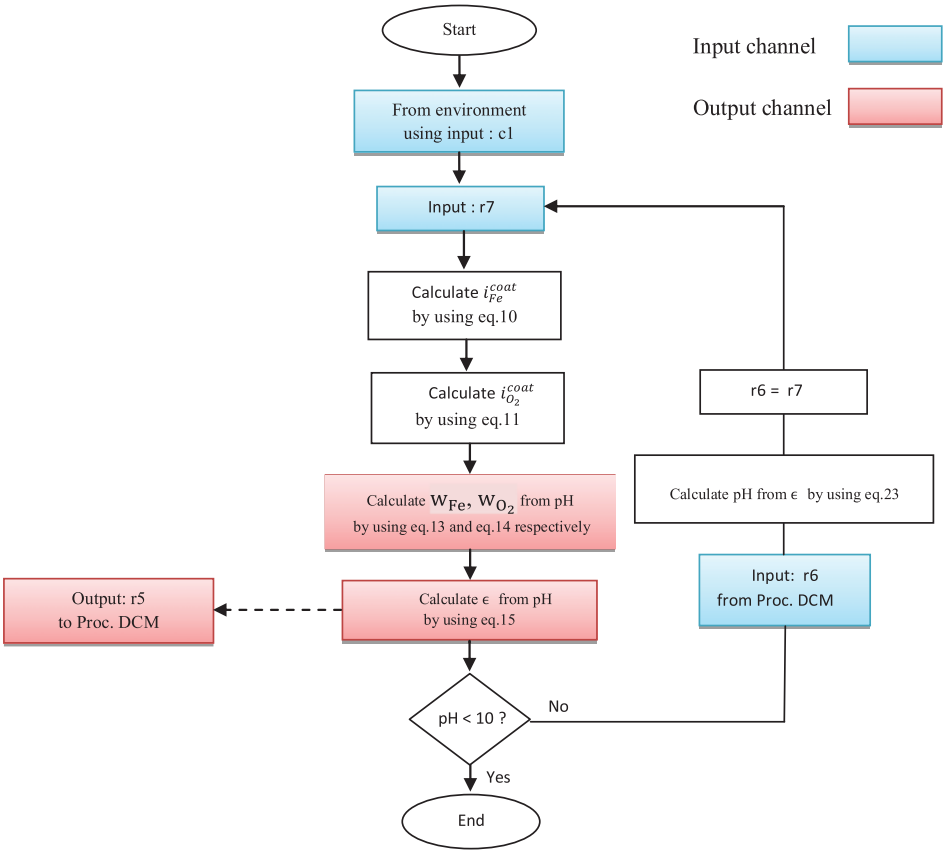

Figure 8. Algorithm for process IPM (Proc. IPM).

Table 6. I/O channels for Proc. IPM with their corresponding signal list.

Input channels		Output channel	
*r*6 (from Proc. DCM) *c*1 *r*7 (from environment)	sig n, sig F, sig D_O, sig c_{O_2}, sig pH, sig ε_c, sig ε_m, sig g_m, sig g_c	*r*5 (to Proc. DCM)	sig ε

Note: Input channel ; Ouput channel .

4.4. Process DCM implementation

The algorithm for process DCM (Proc. DCM) is shown in Figure 9. The I/O channels with signal lists are shown in Table 7. Proc. DCM is used to find the time-dependent ionic concentration $\frac{\partial c_s}{\partial t}$ along the metal-coating interface. The time-dependent ionic concentration $\frac{\partial c_s}{\partial t}$ represents the rate of delamination along the metal-coating interface.

For input channel *r*3 from proc. CTM; sig T, sig RH and sig t_{exp} are the initial values for input signals at the start of simulation run before the iteration process is applied. The input channel *r*5 corresponds to the input from proc. IPM with signal list as: sig ε. The output channel *r*4 corresponds to the signal value sig, $\frac{\partial c_s}{\partial t}$ which

represents the rate of delamination along the metal-coating interface and is used as a final output of proc. DCM and also for the block CDB. The outputs from Proc. DCM, using channels r^2 and $r6$ are fed into proc. CTM and Proc. IPM, respectively, with their respective iterated (processed) parameters.

In analytical modelling, Runge–Kutta (RK-4) method provides with an iterative approach for the effective solution of ordinary PDE. Consider the solution of vector z at time state $t = t_o + h$ as,

$$\frac{dz}{dx} = f(z), \quad z = z_o \text{ at } x = x_o \tag{24}$$

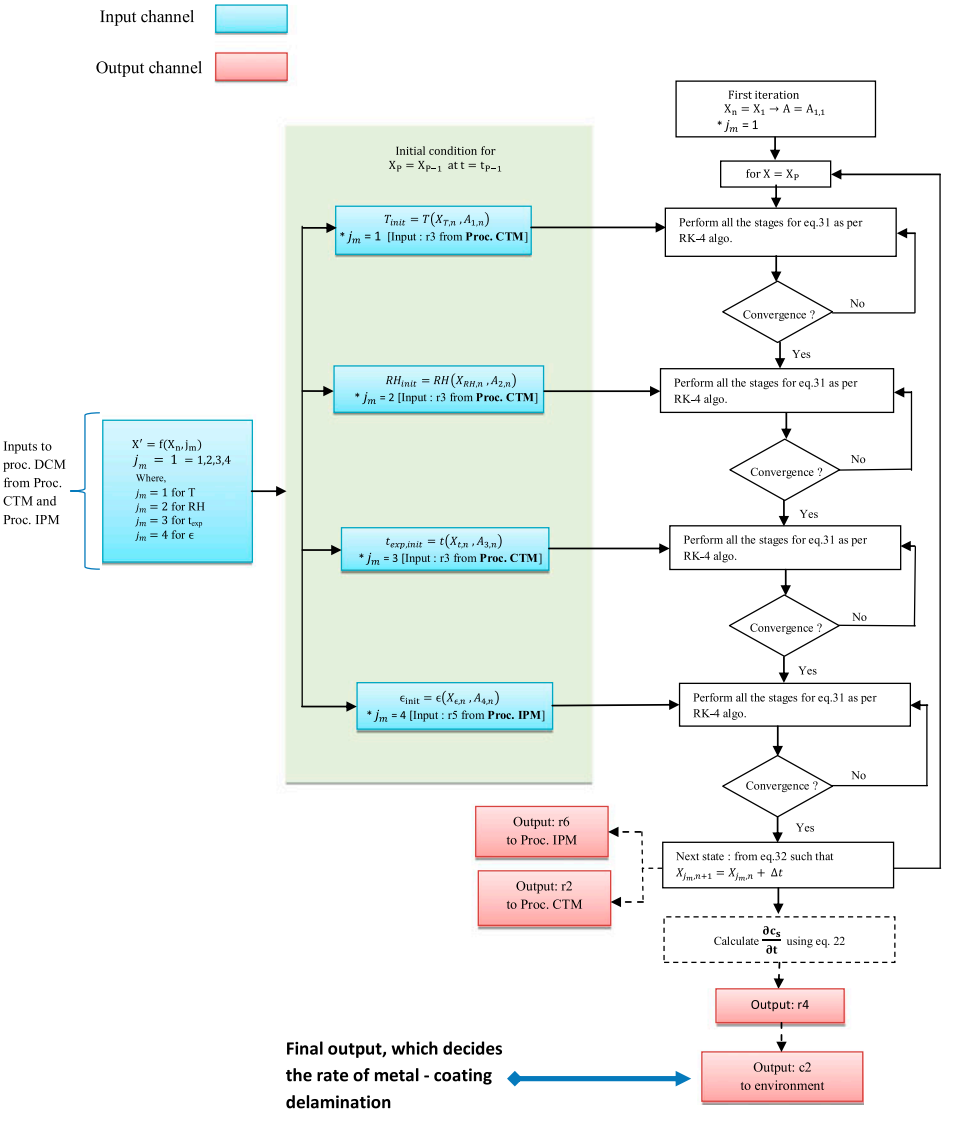

Figure 9. Algorithm for process DCM (Proc. DCM).

Table 7. I/O channels for Proc. DCM with their corresponding signal list.

Input channels		Output channels	
*r*3 (from Proc. CTM)	sig T, sig RH, sig t_{exp},	r^2 (to Proc. CTM)	sig T_i, sig RH_i, sig $t_{exp\ i}$
*r*5 (from Proc. IPM)	sig ε	*r*4 *c*2 (to environment)	sig $\frac{\partial c_s}{\partial t}$
		*r*6 (to Proc. IPM)	sig ε_i

Note: Input channel ; Ouput channel .

where vector z comprises n parameters and the term $f(z)$ represents the way to write a specific function for these parameters.

The PDE (Equation (22)) for the ionic concentration along the interface is solved by utilising RK-4 method. Some symbols have been developed in order to model a PDE in Equation (22). The concentration along the interface of ionic species such as Fe^{2+}, Na^{+} and OH^{-} is influenced by variable parameters: T, RH, t_{exp} and ε. Therefore, the equations for three set of variable parameters, each for Fe^{2+}, Na^{+} and OH^{-} can be written as,

$$X_{Fe} = f_{Fe}(T, RH, t_{exp}, \varepsilon) \tag{25}$$

$$X_{Na} = f_{Na}(T, RH, t_{exp}, \varepsilon) \tag{26}$$

$$X_{OH} = f_{OH}(T, RH, t_{exp}, \varepsilon) \tag{27}$$

The three set of Equations (25)–(27) can be summarised in a vector form as,

$$\overline{X'_{c_s}} = \overline{f_{c_s}}(\overline{X}); \quad \overline{f_{c_s}} = (f_{Fe}, f_{Na}, f_{OH}) \tag{28}$$

where $\bar{X} = (T, RH, t_{exp}, \varepsilon)$ and $\bar{f}_{c_s} = (f_{Fe}, f_{Na}, f_{OH})$. The variable parameter ε is the input from Proc. IPM while variable parameters T, RH and t_{exp} are the inputs from Proc. CTM. The time states are labelled as which are separated by the time step h. $\overline{X_{T,n}}, \overline{X_{RH,n}}, \overline{X_{t_{exp},n}}, \overline{X_{\varepsilon,n}}$ are the values for temperature, relative humidity, time of exposure t_{exp} and ε at time t_n.

$$\overline{X_n} = \overline{X_{T,n}}, \overline{X_{RH,n}}, \overline{X_{t_{exp},n}}, \overline{X_{\varepsilon,n}} \tag{29}$$

$$\overline{X_{n+1}} = \overline{X_{T,n+1}}, \overline{X_{RH,n+1}}, \overline{X_{t_{exp},n+1}}, \overline{X_{\varepsilon,n+1}} \tag{30}$$

Equation (30) accounts for the state X_{n+1} for all the four variable parameters (T, RH, t_{exp}, ε) at time state t_{n+1}.Consider a state X_n at the time t_n. The method computes the next state X_{n+1} at time t_{n+1} after a short-time jump h between the two states i.e. X_n and X_{n+1}. The updated results of variable parameters are stored in the forthcoming state X_{n+1}. This research employs RK-4 method as a platform to solve PDE's in order to run iterative simulation algorithm to quantify delamination rate (due to ionic concentration change along the interface). RK-4 method uses weighted average concept for time iterations. This concept comprises the weighted average sum of four incremental steps with each step as the product of size of interval h (in this research $h/2$).

$$\left.\begin{array}{c}\overline{a_{j_m,n}} = \overline{f_{j_m}}\left(\overline{X_{T,n}}, \overline{X_{RH,n}}, \overline{X_{t_{exp},n}}, \overline{X_{\varepsilon,n}}\right) \\ \overline{b_{j_m,n}} = \overline{f_{j_m}}\left(\left(\overline{X_{T,n}} + \frac{h}{2}\bar{a}_{1,n}\right), \left(\overline{X_{RH,n}} + \frac{h}{2}\bar{a}_{2,n}\right), \left(\overline{X_{t_{exp},n}} + \frac{h}{2}\bar{a}_{3,n}\right), \left(\overline{X_{\varepsilon,n}} + \frac{h}{2}\bar{a}_{4,n}\right)\right) \\ \overline{c_{j_m,n}} = \overline{f_{j_m}}\left(\left(\overline{X_{T,n}} + \frac{h}{2}\bar{b}_{1,n}\right), \left(\overline{X_{RH,n}} + \frac{h}{2}\bar{b}_{2,n}\right), \left(\overline{X_{t_{exp},n}} + \frac{h}{2}\bar{b}_{3,n}\right), \left(\overline{X_{\varepsilon,n}} + \frac{h}{2}\bar{b}_{4,n}\right)\right) \\ \overline{d_{j_m,n}} = \overline{f_{j_m}}\left(\left(\overline{X_{T,n}} + \frac{h}{2}\bar{c}_{1,n}\right), \left(\overline{X_{RH,n}} + \frac{h}{2}\bar{c}_{2,n}\right), \left(\overline{X_{t_{exp},n}} + \frac{h}{2}\bar{c}_{3,n}\right), \left(\overline{X_{\varepsilon,n}} + \frac{h}{2}\bar{c}_{4,n}\right)\right)\end{array}\right\} \quad (31)$$

Four steps incremental process

Thus, next state X_{n+1} is given as,

$$\overline{X_{j_m,n+1}} = \overline{X_{j_m,n}} + \frac{h}{6}\left(\overline{a_{j_m,n}} + \overline{2b_{j_m,n}} + \overline{2c_{j_m,n}} + \overline{d_{j_m,n}}\right) \quad (32)$$

where $j_m = 1$, 2, 3 and 4 in Equations (31) and (32) represent set of four variable parameters: T, RH, t_{exp} and ε. The RK-4 method offers the perfect key to simulate the exposed material boundaries. No flux condition was considered for Cl^- which act as chemically inert species and only the boundary conditions for Fe^{2+}, Na^+ and OH^- are taken into account at the metal surface. For Fe(OH), the equilibrium relationship for both the ionic species are used as boundary condition.

Figure 9 shows the algorithm for evaluating the profile of ionic concentration along one dimension i.e. 'x-axis' along metal-coating interface. The developed algorithm encapsulates and utilises RK-4 method. The algorithm calculates the values of variable parameters for a given time t for every stage with $h/2$ as an incremental time gap. The algorithm in Figure 9 follows the following steps.

(1) Function $\overline{X'_{c_s}} = \overline{f_{c_s}}(X_n, j_m)$ accounts for (3×4) matrix function. Where X_n corresponds to three separate rows, each row for one ionic species: f_{Fe}, f_{Na} and f_{OH} (Equation (28)). j_m corresponds to variable parameters T, RH, t_{exp} and ε with $j_m = 1$, 2, 3, 4, representing T, RH, t_{exp} and ε, respectively.

$$\overline{X'_{c_s}} = \overline{f_{c_s}}\begin{bmatrix} X^{Fe}_{T,n} & X^{Fe}_{RH,n} & X^{Fe}_{t_{exp},n} & X^{Fe}_{\varepsilon,n} \\ X^{Na}_{T,n} & X^{Na}_{T,n} & X^{Na}_{t_{exp},n} & X^{Na}_{\varepsilon,n} \\ X^{OH}_{T,n} & X^{OH}_{T,n} & X^{OH}_{t_{exp},n} & X^{OH}_{\varepsilon,n} \end{bmatrix} \begin{array}{l} \longleftarrow f_{Fe} \\ \longleftarrow f_{Na} \\ \longleftarrow f_{OH} \end{array} \quad (33)$$

(2) From Figure 9, the 'initial condition' (in olive green box) for four different profiles (T, RH, t_{exp}, ε) is set as: $X_p = X_{p-1}$, where P in X_p represent the maximum number of iterations programmed before the start of simulation. $T_{init} = T\left(X_{T,n}, A_{j_m,n}\right)$, $RH_{init} = RH\left(X_{RH,n}, A_{j_m,n}\right)$, $t_{init} = t\left(X_{t,n}, A_{j_m,n}\right)$ $\varepsilon_{init} = \varepsilon\left(X_{\varepsilon,n}, A_{j_m,n}\right)$ represent profiles for all four variable parameters. Input from channel $r3$ corresponds to T, RH and t_{exp} while input from channel $r5$ corresponds to the ε.

(3) In Equation (33), each element of a matrix is treated with RK-4 method. $A_{j_m,n}$ represent a four-step incremental process (Equation (31)) within RK-4 method. $A_{1,n}$, $A_{2,n}$, $A_{3,n}$, $A_{4,n}$ represent four stages within RK-4 method for T, RH, t_{exp} and ε, respectively.

$$\overline{e_{\text{init}}} = f_{\text{init}} \begin{bmatrix} X_{\text{T,n}} & X_{\text{T,n+1}} & X_{\text{T,n+2}} & & X_{\text{T,P}} \\ X_{\text{RH,n}} & X_{\text{RH,n+1}} & X_{\text{RH,n+2}} & \cdots & X_{\text{RH,P}} \\ X_{\text{t}_{\text{exp}},\text{n}} & X_{\text{t}_{\text{exp}},\text{n+1}} & X_{\text{t}_{\text{exp}},\text{n+2}} & & X_{\text{t}_{\text{exp}},\text{P}} \\ X_{\varepsilon,\text{n}} & X_{\varepsilon,\text{n+1}} & X_{\varepsilon,\text{n+2}} & & X_{\varepsilon,\text{P}} \end{bmatrix} \begin{matrix} \longleftarrow A_{1,\text{n}} \\ \longleftarrow A_{2,\text{n}} \\ \longleftarrow A_{3,\text{n}} \\ \longleftarrow A_{4,\text{n}} \end{matrix} \tag{34}$$

where $\overline{e_{\text{init}}}$ is a $(4 \times P)$ matrix function with f_{init} representing the function $(T_{\text{init}}, \text{RH}_{\text{init}}, \text{t}_{\text{init}}, \varepsilon_{\text{init}})$ for the initial conditions. Simulation ends when the number of iterations/states n performed by algorithm become equal to the number of iteration programmed before the simulation run i.e. $n = P$.

(4) Simulation starts with the first iteration considering an initial condition $X_{\text{n}} = X_1 \rightarrow A = A_{1,1}$. The terms j_{m} and n in $A_{j_{\text{m}},\text{n}}$ are both set equal to 1 as simulation starts by considering the temperature profile at first and then moving to the next profiles. The simulation performs the four-step incremental process (RK-4) for the current profile and moves to the next profile if the given convergence criterion is reached.

$$\left[\frac{\Phi^{\text{r+1}}_{\text{j}_{\text{m}},\text{n}} - \varphi^{\text{r}}_{\text{j}_{\text{m}},\text{n}}}{\Phi^{\text{r}}_{j_{\text{m}},\text{n}}} \right] \leq \mu \tag{35}$$

where $\Phi^{\text{r}}_{\text{j}_{\text{m}},\text{n}}$ represents the n^{th} iteration. Each iteration increments after performing four-step incremental process for the j^{th}_{m} variable (T, RH, t_{exp},) ε. Each step of the four steps (a,b,c,d) incremental process is represented by the term r in Equation (35). The convergence criterion μ is set initially before the start of simulation.

(5) Proc. DCM calculates the ionic concentration $\frac{\partial c_{\text{s}}}{\partial t}$ (using Equation (22)) after the every state/iteration using the updated values of T, RH, t_{exp} and ε. Proc. DCM outputs the value of sig $\frac{\partial c_{\text{s}}}{\partial t}$ using channel $r4$. The output value from channel $r4$ is then sent as an output value to the environment using channel $c2$. The output value of $\frac{\partial c_{\text{s}}}{\partial t}$ is the final value which decides the rate of metal-coating delamination. Similarly, after every state/iteration, DCM outputs the (processed) values of T, RH, t_{exp} and ε using channels $r6$ and r^2. The channels $r6$ and r^2 are set to feed the (processed) values (as input values) to Proc. IPM and Proc. CTM, respectively.

5. Simulation results and discussion

The purpose of this work is to develop an accurate and an efficient approach to simulate the propagation of metal-coating delamination. This section accounts for the simulation results and an explanation for the results of cathodic delamination system. The 'metal-coating delamination rate' can be analysed from the ionic concentration (mol/cm^3) along the metal-coating interface. This ionic concentration is obtained as a final output from Proc. DCM via. channel $c2$ as shown in Figure 10. The concentration profile for various ionic concentrations (Fe^{2+}, Na^+ and OH^-) along the interface is shown for $t = 0.125$ s. The detailed timely analysis of all the parameters which are involved in the metal-coating delamination is explained in the following sections.

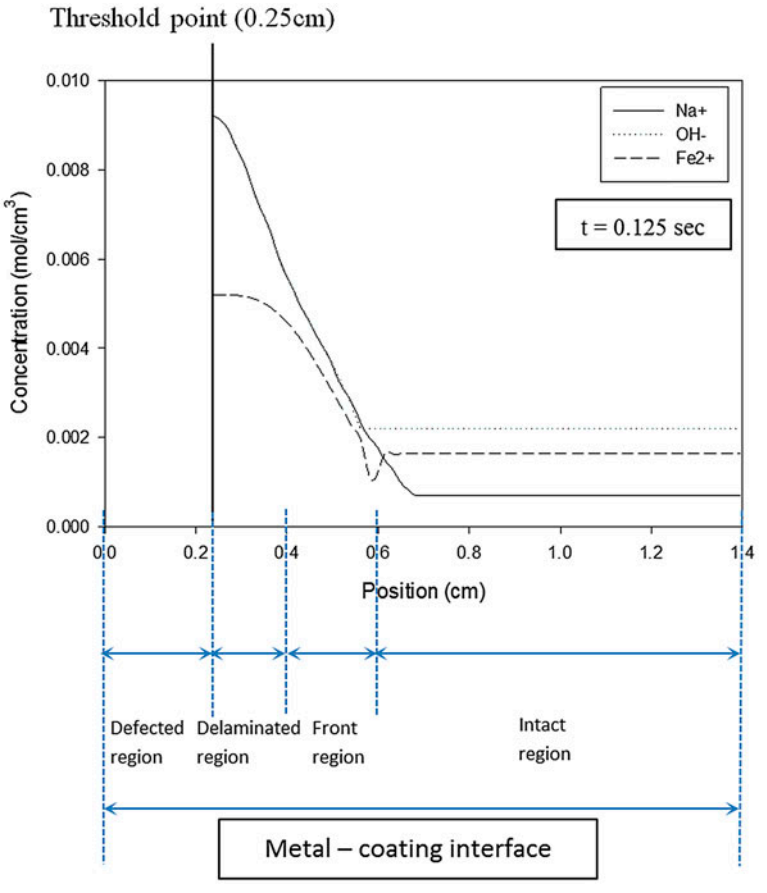

Figure 10. Final output from Proc. DCM via channel *c*2.
The trends in this graph are used to analyse the metal-coating delamination rate along the interface. The graph also define the physical boundaries along the interface.

5.1. Initial conditions

The initial conditions are: (i) Metal-coating interface has the physical boundaries for various regions of delamination along the interface. These physical boundaries are shown in Table 8 and Figure 10. (ii) The developed model accounts for the timely variation of delamination parameters instead of variation of physical boundaries which are considered to be fixed. (iii) The electrolyte potential is assumed to be negligible ($\Phi_B = 0$) at the bulk condition. Φ follows the electro neutrality condition at all the boundaries including fully intact region. (iv) The coating defect is set at position $x = 0$ along the two-dimensional plane. The concentration of cation (e.g. Na^+) and species produced due to electrochemical reactions at position $x = 0$ are set equal to 0 mol. (v) The threshold position along the interface for any cation is set equal to $x = 0.25$ cm with different threshold concentration values for each species as shown in Figure 10. (vi) The delaminated boundary at $x = 0.25$ cm is reported to be highly alkaline with the initial concentration $c_{Na+} = 0.009$ mol. It is assumed that in the delaminated (porous) region $c_{Na+} \approx c_{OH^-}$. The value of the concentration for each species declines along the position axis other than Fe^{2+} which is accustomed to maintain the electro neutrality condition as shown in Figure 10.

Table 8. Boundary allocation for various regions along the delaminated metal-coating interface used in simulation.

Defected region (scratch) (cm)	Delamination region (cm)	Front region (cm)	Intact region (cm)
0.0–0.25	0.25–0.4	0.4–0.6	0.6–1.4

5.2. Geometric parameters

The geometric parameters along with other delamination parameters are used to define the electrochemistry involved in the CDB. The delamination parameters are characterised in the form of signal list. These signals are declared inside the block CDB and are defined as input or output signals using channels. These channels along with the specific signal list are used to communicate between the processes: proc. CTM, proc. DCM and proc. IPM.

The delamination parameters which are used as inputs for proc. IPM include a signal list as: sig g_c, sig g_m with values as 35 and 5 μm, respectively. The signal for diffusion coefficient value of any ionic species is defined as sig $D_{S,STA_{ion}}$ (shown in Table 2). The signals for diffusion coefficients for oxygen O_2, OH^-, Fe^{2+} are defined as sig D_{O_2}, sig $D_{OH^-,STA}$ and sig $D_{Fe^{2+},STA}$, respectively. Where $D_{O_2} = 2 \times 10^{-5}$ cm^2/s, $D_{OH^-,STA} = 6.1 \times 10^{-7}$ cm^2/s and $D_{Fe^{2+},STA} = 0.5 \times 10^{-7}$ cm^2/s. sig $c_{O_2} = 1.3 \times 10^{-3}$ mol represents signal of the dissolved concentration of oxygen at coating surface. The polarisation parameters i.e. Tafel slope, exchange current density and equilibrium potential for iron dissolution are: $\beta_{Fe2+} = 0.41$ V/decade, $i_{0,Fe} = 7.1e^{-3}$A/cm^2 and $E_{0,Fe} = -0.409V_{SHE.}$ The grid size for graphical analysis is set equal to 0.0254 cm and time step h is 0.012 s. The net length for the metal-coating interface (including delamination, front and intact regions) is set equal to 1.4 cm.

5.3. Process CTM simulation results

The simulation results for Proc. CTM are presented in this section.

5.3.1. Concentration distribution (c_{Na^+})

CTM algorithm starts with the condition, $c_B = c_{Na+}$ assuming that the concentration along the interface is equal to bulk concentration at metal-coating defect upon condition that the distance to the defect is greater than zero and average ionic species diffusion time is zero. CTM simulates till condition i.e. $c_{Na+} = 0$ is met assuming that the bulk Na^+ concentration along the interface becomes zero. The initial values for T, RH and t_{exp} are set as standard values and iterative values along the course of time are used as input signal list from DCM which effect the standard diffusion coefficient parameter. The percentage change for each iterative value (T_i, RH_i, $t_{exp,i}$) is kept small in order to study the close relationship for concentration change c_{Na+} along the interface. The calculated distribution of c_{Na+} along the interface for 35 min is shown in Figure 11(a).

5.3.2. Flux distribution (N_{Na^+})

The flux distribution of Na^+ with the position along the interface is shown in Figure 11(b). The diffusion process is facilitated by the negative concentration gradient of Na^+ ions. The positive flux value N_{Na^+} implied the net transport of Na^+ into the delaminated region. The value of N_{Na^+} decreases along with the time inside the delaminated and the front

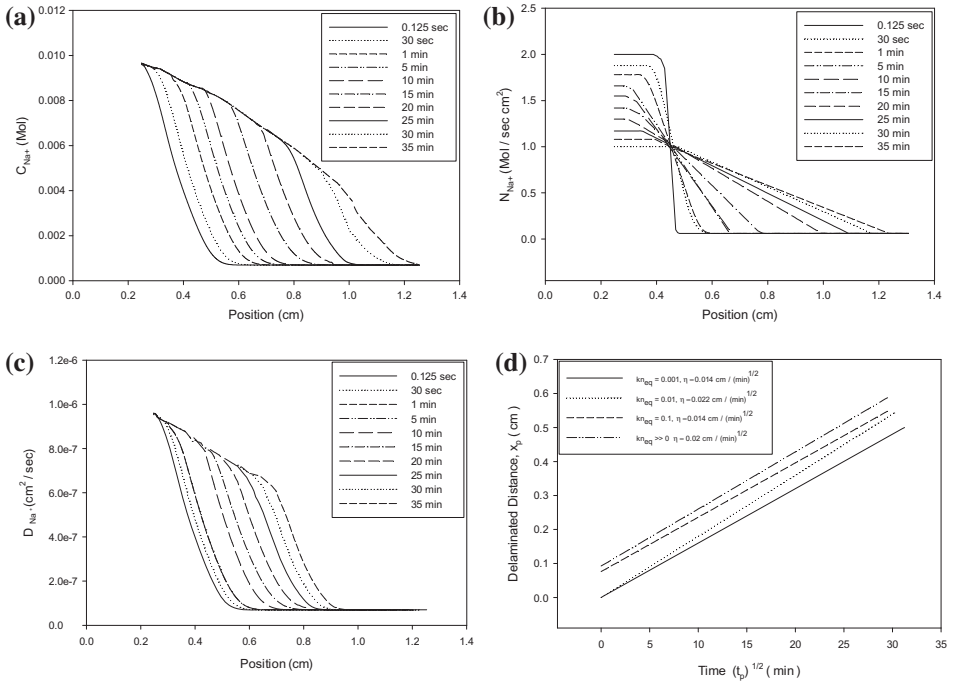

Figure 11. Graphical representation of CTM simulation results of various delamination rate measuring parameters: (a) concentration distribution of sodium along the interface, (b) flux distribution, (c) diffusivity distribution and (d) delaminated distance w.r.t time as a function of rate constant.

region (<0.6 cm) but continued to increase in the intact region (>0.6 cm). The results for the change in flux are consistent with Allahar's results in terms of decreasing profile with the passing time. But for the concentration (in Section 5.3.1), a more dramatic fall is observed during 35 min. simulation time.

5.3.3. *Diffusivity distribution (D_{Na+})*

The diffusivity profile for the sodium D_{Na+} is shown in Figure 11(c). The initial values for T, RH and t_{exp} are set equal to standard values and change in the values due to iterations with the passing time is set to be very small in order to observe the close relationships for various cationic parameters like c_{Na+} (in Section 5.3.1), N_{Na+} (in Section 5.3.2). The value of D_{Na+} is found to be negligible inside the intact region. Conventional models did not consider the variation in D_{Na+} along the course of time with varying T, RH and t_{exp} which are important parameters and need to be considered because of their key role in diffusion rate and eventually concentration and flux distribution along the interface.

5.3.4. *Potential front slope η vs. rate reaction for the bond breakage (kn_{eq})*

The delaminated distance with respect to time in min. as function of rate constant kn_{eq} is shown in Figure 11(d). The rate constant kn_{eq} is assumed to vary from $1e^{-3}$ s^{-1} to a

very large value (>> 0) with the change in the slope (η) of delaminated distance line from 0.014 to 0.02 cm/(min)$^{1/2}$, respectively. This small variation in slope shows that the rate constant has a very small effect on the rate-determining step of the overall delamination process. Huang's [17] simulation results showed significant variation in slope from 0.57 to 0.59 irrespective of the same variation in rate constant from $1e^{-3}$ s^{-1} to a very large value. However, Huang's and the developed model simulation results are consistent in a way that the slope of the line increases with the increase in rate constant.

5.4. Process IPM simulation results

The simulation results for Proc. IPM are presented in this section.

*5.4.1. Potential distribution (*V*), potential gradient (d*V*/d*x*) and potential front*

The graphical representation for the simulation results for the interfacial potential of 35 min. simulation study is shown in Figure 12(a). An exponential rise is observed in the interfacial potential away from the defected region (e.g. scratch) and shows a constant behaviour inside the intact region. The profile shape for the interfacial potential remains the same; however, a slight increase in the potential along the interface is observed with respect to time. The results are consistent with the Leng and Stratmann's

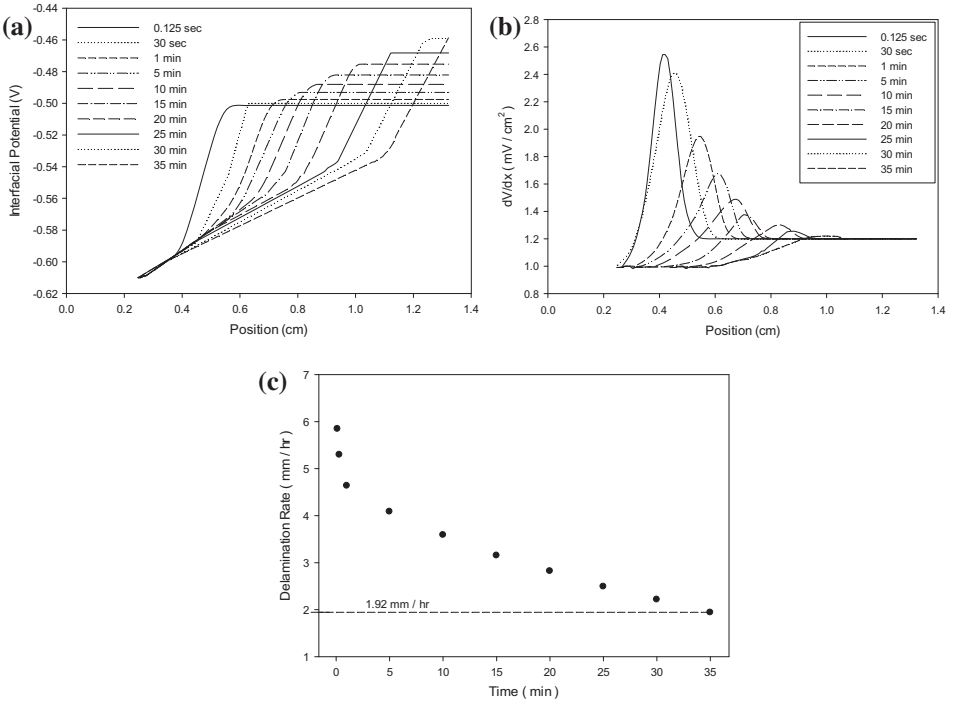

Figure 12. Graphical representation of IPM simulation results of various delamination rate measuring parameters: (a) interfacial potential along metal-coating interface, (b) potential gradient and (c) delamination rate showing the instantaneous potential front velocity.

[9,11] experimental results but the interfacial potential values are found to be almost 50 and 20% in magnitude as reported by Allahar and Huang [16,17] in their simulation study, respectively. The interfacial potential is differentiated with respect to time in order to yield potential gradient (dV/dx). These differentiation results are plotted as spikes of potential with decreasing height along with increasing time as shown in Figure 12(b). The height of each spike showed the magnitude of potential gradient (dV/dx). These graphical results for dV/dx are also consistent with Leng and Stratmann's [9,11] experimental results. However, the results show the difference in the values when compared with Allahar's and Huang's [16,17] results. This difference in results for dV/dx is the same as observed for interfacial potential (Figure 12(a)). This decaying behaviour in spikes height is due to the gradual decrease in the electrochemical potential with increasing time. The propagation rate for the potential front is calculated from the maxima of the spikes given in Figure 12(b) which also represents delamination rate as shown in Figure 12(c). The delamination rate decreases exponentially with time. The calculated delamination rate (1.92 mm/h) for the front end is found to be much consistent with Allahar's [16] simulation results (2.153 mm/h) compared to Huangs [17] simulation results (1.66 mm/h). However, experimental delamination rate quoted by Leng and Stratmann [9,11] is twice smaller compared to delamination rate calculated by the developed model.

5.4.2. *Oxygen reduction current density ($i_{O_2}^{coat}$) and pH distribution*

The simulation results showed a small increase in the electrochemical reactivity along the metal-coating interface with the propagation of delamination front into the intact region. The oxygen reduction due to electrochemical reactivity results in the production of OH^-, as can be seen in Figure 13(a). A small sharp increase in the value of $i_{O_2}^{coat}$ states the sudden rise in the current due to electrochemical reactivity. The current density falls to the minimum value inside the intact region. This production of OH^- due to oxygen reduction indicates the increase in pH in the delaminated and front regions. The trend of pH distribution along the interface with the passing time is shown in Figure 13(b). There is a difference of 13% in the calculated results for current density $i_{O_2}^{coat}$ from the results reported by Allahar [16]. However, the pH values are found to be almost similar to Allahar's [16] and Huang's [17] simulation results.

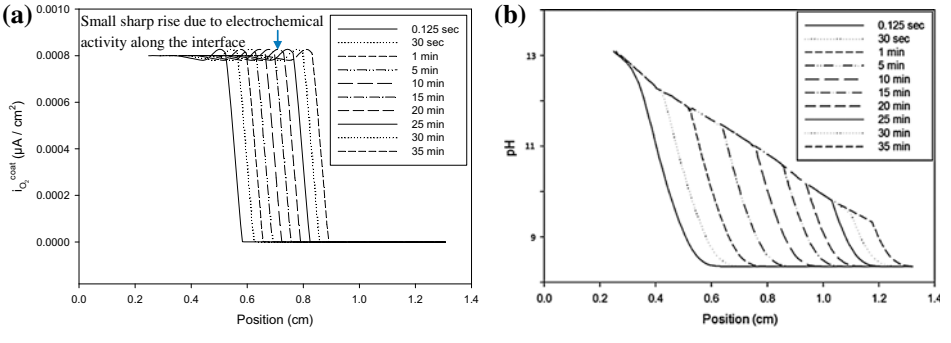

Figure 13. Graphical representation of IPM simulation results of various delamination rate measuring parameters: (a) oxygen reduction current density along the metal-coating interface and (b) pH distribution.

5.4.3. pH gradient (dpH/dx) and pH front

The profile trend for pH gradient along the interface with the course of time is shown in Figure 14(a). The shape follows the same trend as calculated for dV/dx (Figure 12(b)). These values are calculated using equilibrium rate constant value i.e. $kn_{eq} \gg 0$. The values of pH front calculated from the deflection points in pH gradient profile are used for the calculation of 'velocity of pH front' are shown in Figure 14(b). The velocity front is found to be equal to 2.02 mm/h which is 16.3 % greater than the value reported by Huang [17] while Allahar [16] did not report the results for pH gradient and pH velocity front.

5.4.4. Polarisation parameters (w_{O_2} and w_{Fe})

The polarisation parameters; w_{O_2} and w_{Fe} are dependent upon the pH as clear from Equation (13) to Equation (14), respectively. The equilibrium rate constant $kn_{eq} = \infty$ is used throughout this simulation study. This rate constant value is also considered for the calculation of values for the other parameters like pH and porosity. However, a comparison study with non-equilibrium rate constant values will be made in Section 5.6. The distributions for w_{O_2} and w_{Fe} are shown in Figure 15(a) and (b), respectively. These polarisation parameter values are almost found to be consistent with the simulation values reported by Allahar [16] while Huang [17] did not report the polarisation parameter distribution along metal-coating interface.

5.5. Process DCM simulation results

The simulation results for Proc. DCM are presented in this section.

5.5.1. Porosity distribution (ε)

The graphical representation of the result for porosity distribution along the interface is shown in Figure 16(a). The profile shape for porosity distribution is found to be almost the same as the pH distribution in Figure 13(b) illustrates the fact that both the parameters directly relate to the production of OH^- ions as a result of electrochemical reaction.

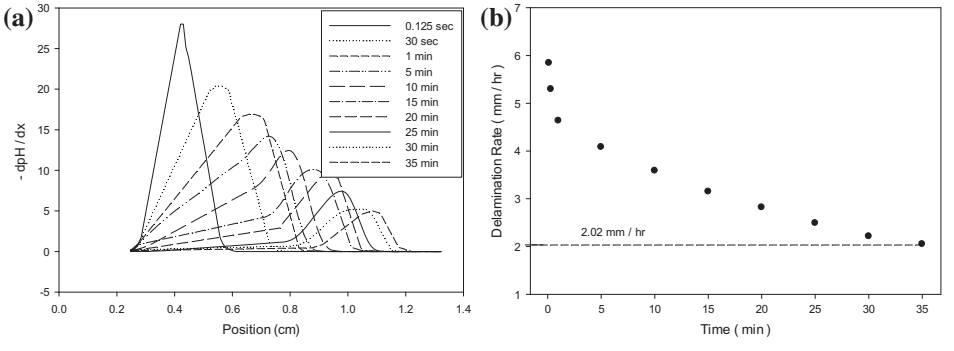

Figure 14. Calculated distribution of (a) pH gradient and (b) velocity of pH front.

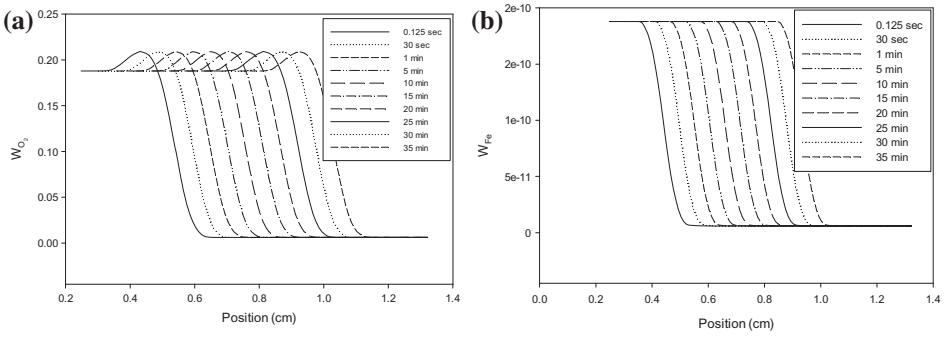

Figure 15. Calculated distribution of polarisation kinetics parameters along the metal-coating interface: (a) w_{O_2} and (b) w_{Fe}.

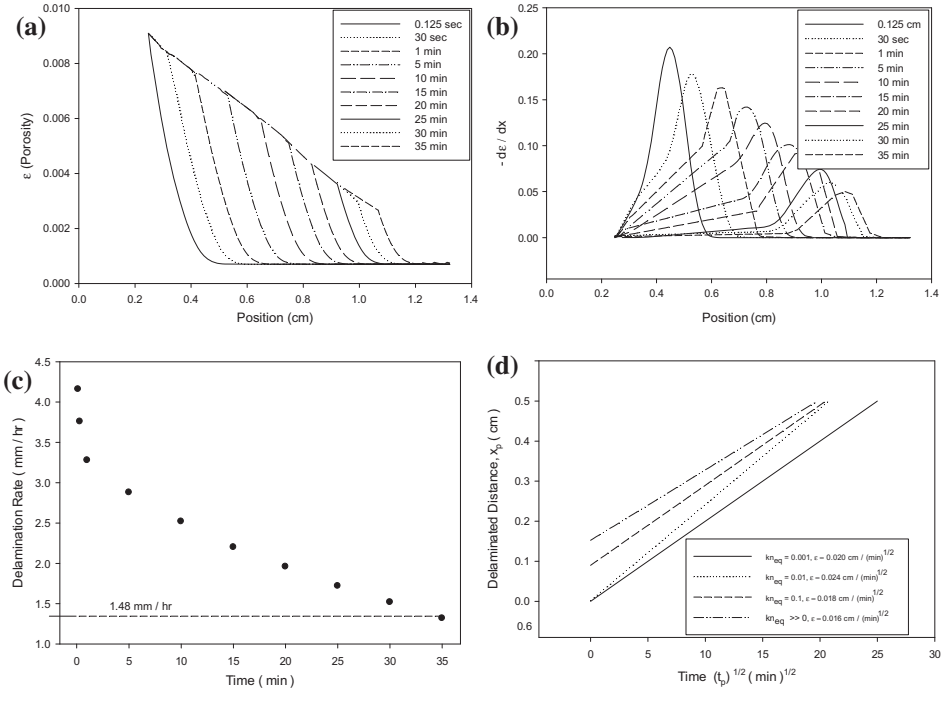

Figure 16. Graphical representation of DCM simulation results of various delamination rate measuring parameters: (a) porosity distribution (b) porosity gradient (c) porosity front (d) delamination rate showing the instantaneous porosity front velocity.

5.5.2. Porosity gradient (dε/dx) and porosity front

Apart from the delamination front velocity as shown in Figure 12(c), instantaneous front velocity can also be represented by taking maxima of porosity gradient as shown in Figure 16(b) and (c). The porosity gradient profile dε/dx along the metal-coating interface with the passing time is shown in Figure 16(b). The maxima of each spike for the porosity gradient profile denotes the porosity front which is eventually used for

the calculation of interfacial front velocity which illustrates the delamination rate as shown in Figure 16(c). Thus, apart from potential front, porosity front is also used to calculate the front velocity. It is more reasonable to define front velocity in terms of porosity front as porosity is the key parameter to measure metal-coating bonding. The value of porosity front in Figure 16(c) is much closer to the value reported by Huang [17] compared to Allahar's [17].

5.5.3. *Porosity front slope* η *vs. rate reaction for the bond breakage* (kn_{eq})

The simulation graph for the porosity front slope η as a function rate reaction of bond breakage with respect to passing time is shown in Figure 16(d). The calculated slope is found to be approximately equal to 0.016 cm/min$^{1/2}$ at an equilibrium rate constant (>> 0) but increases to 0.024 cm/min$^{1/2}$ at 1e^{-3}/s. This shift in the slope is attributed to the limited mass transfer that results in sufficiently slow bond breakage reaction. The results are almost consistent with Huang's [17] simulation results and Strattman's [9,11] experimental results. Allahar [16] did not reportd porosity front slope results.

5.5.4. *Flux distribution* (N_{OH^-})

The flux distribution due to OH^- is shown in Figure 17(a). The flux distribution N_{OH^-} decreases inside the front region and is found to be negligible inside the intact region. However, a sudden slight increase in the value of N_{OH^-} is observed with respect to time. However, the trend for N_{OH^-} decreases with respect to position along the interface. The results for N_{OH^-} are found to be almost consistent with Allahar's [16] simulation results. Huang [17] did not report the flux distribution simulation results.

5.5.5. *Diffusivity variations* (D_{OH^-} *and* $D_{Fe^{2+}}$)

The diffusivity profile for the oxygen and iron; D_{OH^-} and $D_{Fe^{2+}}$ is shown in Figure 17(b) and (c), respectively. As diffusion is dependent upon T, RH, t_{exp}; the initial values for T, RH and t_{exp} are set equal to the standard values and change in the values due to iterations with the passing time are set to be very small in order to observe the close relationship for N_{OH^-} simulation values. The values of D_{OH^-} and $D_{Fe^{2+}}$ are found to be negligible inside the intact region. Conventional models did not consider the variation in D_{OH^-} and $D_{Fe^{2+}}$ along the course of time with varying T, RH and t_{exp}. The variation in diffusivity due to gradual variation in T, RH and t_{exp} directly affect the concentration and flux distribution values along the interface.

5.6. *Comparison of equilibrium and non-equilibrium relationships for various parameters*

To explore the role of rate constant kn_{eq} over equilibrium and non-equilibrium behaviour of various parameters, different values of kn_{eq} are examined as shown in Figures 18–23. A series of simulations are examined for various values of kn_{eq} however, for the purpose of comparison study only two values are presented i.e. $kn_{eq} = 10^{-2}$ and 10^{-1}/s.

The interfacial potential distribution for $kn_{eq} = 10^{-1}$/s and $kn_{eq} = 10^{-2}$/s with the passing time is shown in Figure 18(a) and (b), respectively. The plot for graph in Figure 18(a) is almost similar to the one shown in Figure 12(a). The plot in Figure 12(a)

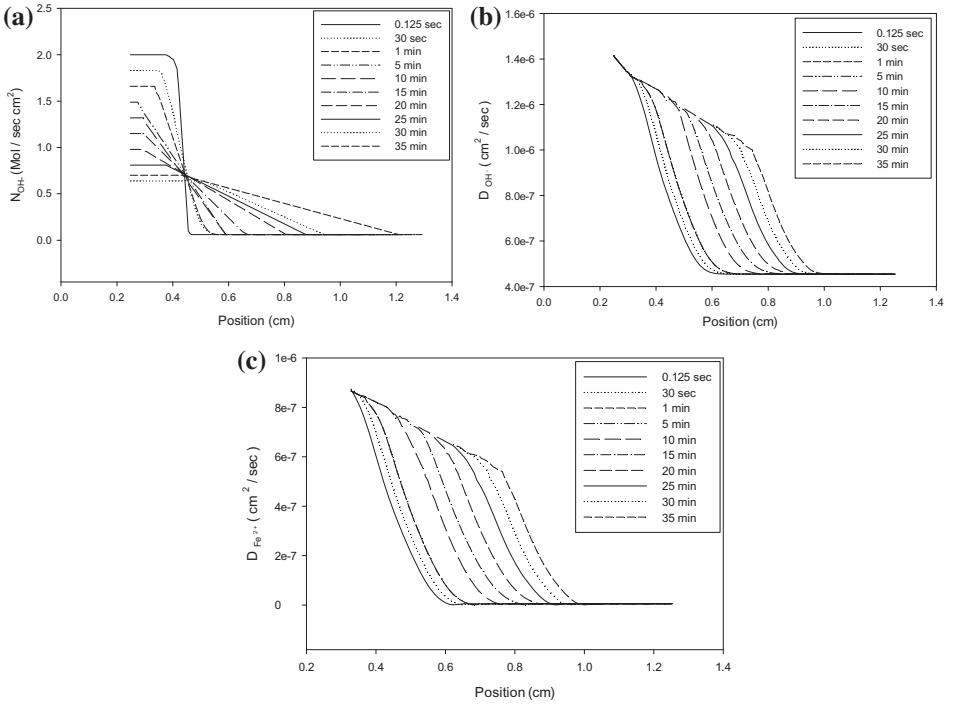

Figure 17. Graphical representation of DCM simulation results of various delamination rate measuring parameters: (a) flux distribution of OH^- ions, (b) diffusivity distribution of OH^- ions along the interface and (c) Diffusivity distribution of Fe^{2+} ions along the interface.

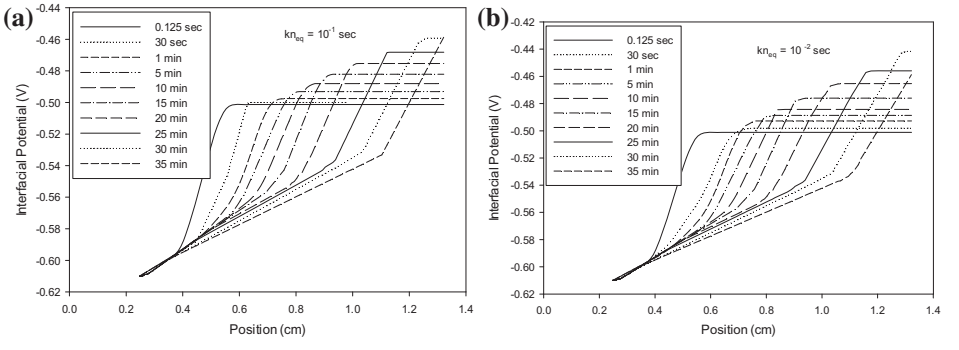

Figure 18. Interfacial potential distribution along the metal-coating interface with passing time (a) $kn_{eq} = 10^{-1}$/s and (b) $kn_{eq} = 10^{-2}$/s.

is plotted considering equilibrium rate constant condition $kn_{eq} \gg 0$. However, the graph changes its features as the value of kn_{eq} progresses, until it reaches non-equilibrium state. The potential gradient distribution for equilibrium and non-equilibrium relationship is shown in Figure 19(a) and (b). The plot for $kn_{eq} = 10^{-1}/s$ is almost the same as Figure 12(b). The delamination rate determined by potential front values are found to be

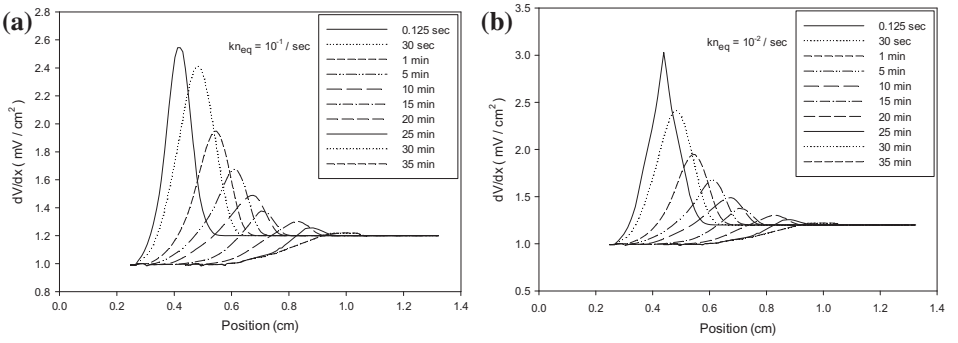

Figure 19. Potential gradient distribution along the metal-coating interface with passing time (a) $kn_{eq} = 10^{-1}$/s and (b) $kn_{eq} = 10^{-2}$/s.

1.86 and 1.61 mm/h for $kn_{eq} = 10^{-1}/s$ and for $kn_{eq} = 10^{-2}/s$, respectively. This variation in porosity front indicates that the rate constant kn_{eq} directly affects the delamination rate.

The porosity distribution with elapsed time as a parameter is shown for 10^{-1}/s and 10^{-2}/s in Figure 20(a) and (b).The porosity profile is much evident in Figure 20(a) compared to Figure 20(b) which suggest that with lower values of kn_{eq} the porosity decreases in a much sharper manner compared to higher values of rate constant. In Figure 21(b), the rate constant kn_{eq} is set to $10^{-3}/s$ instead of $10^{-2}/s$ to illustrate the clear sharp decrease in porosity value with time lapse. Figure 21(a) and (b) shows the porosity gradient for $kn_{eq} = 10^{-1}/s$ and $kn_{eq} = 10^{-2}/s$, respectively. For $kn_{eq} = 10^{-2}/s$, a gradual increase in the porosity value is observed in a region with high electrochemical activity or high pH i.e. the front region.

Figure 22(a) and (b) shows pH distribution along the interface for 10^{-1}/s and 10^{-2}/s, respectively. For $kn_{eq} = 10^{-2}/s$, the pH distribution is more converged inside the intact region compared to $kn_{eq} = 10^{-1}/s$. The pH gradient profile in Figure 23(a) and (b) shows a close behaviour with dV/dx in Figure 19(a) and (b). The pH front velocities calculated from Figure 23(a) and (b) are 1.95 and 1.62 mm/h, respectively. Both the values relate closely with the potential front velocities for equilibrium and non-equilibrium

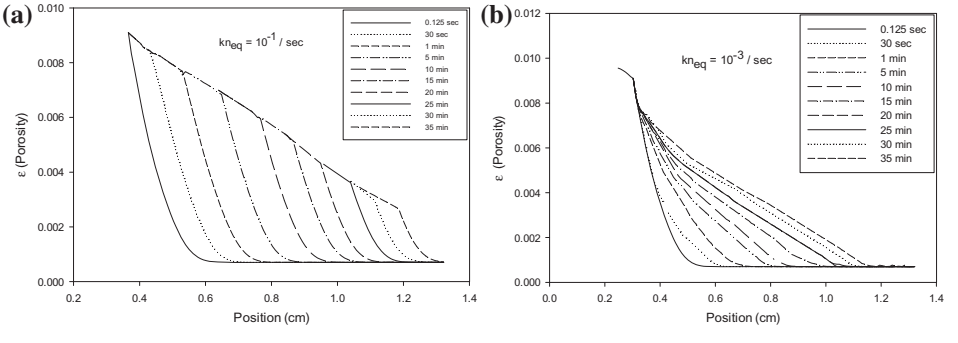

Figure 20. Porosity distribution along the metal-coating interface with passing time (a) $kn_{eq} = 10^{-1}$/s and (b) $kn_{eq} = 10^{-3}$/s.

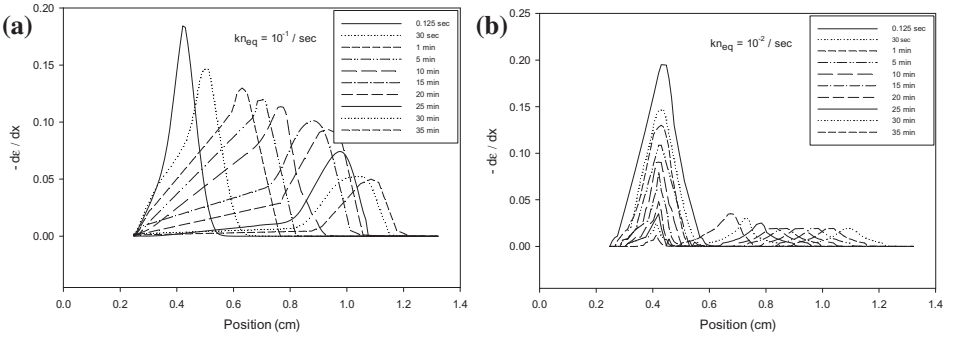

Figure 21. Porosity gradient distribution along the metal-coating interface with passing time (a) $kn_{eq} = 10^{-1}$/s and (b) $kn_{eq} = 10^{-2}$/s.

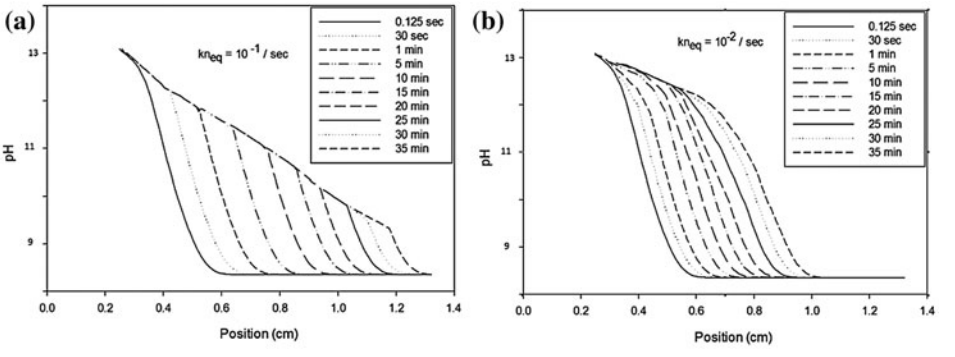

Figure 22. pH distribution along the metal-coating interface with passing time (a) $kn_{eq} = 10^{-1}$/s and (b) $kn_{eq} = 10^{-2}$/s.

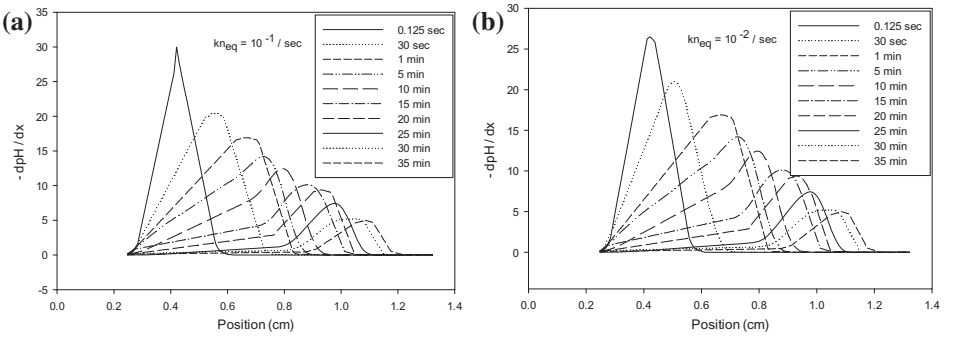

Figure 23. pH gradient distribution along the metal-coating interface with passing time (a) $kn_{eq} = 10^{-1}$/s and (b) $kn_{eq} = 10^{-2}$/s.

states. This decrease in pH front velocity value can be attributed to lower porosity in the region. Porosity of the region directly relates with electrochemical activity resulting in OH^- ions production and also the ionic diffusivity.

5.7. Sensitivity analysis of the fitting parameters

The fitting parameters for ε–pH, V–pH, w_{O_2}–pH, w_{Fe}–pH relations can seriously affect the simulation results. These fitting parameters decide the shape of overall pH, porosity and polarisation parameter curves. So, a beforehand accurate computation of these parameters is required to get precise simulation results. The analysis is performed using three different values for each parameter against each relation.

The simulation curves of ε–pH relationship for various fitting parameter values $(b_{\varepsilon,1} - b_{\varepsilon,3})$ are shown in Figure 24(a).When the fitting parameter $b_{\varepsilon,1}$ increases from 0.001 to 0.1 the porosity value also increases resulting in the increase in porosity front velocity and also increasing the potential front velocity because of their direct

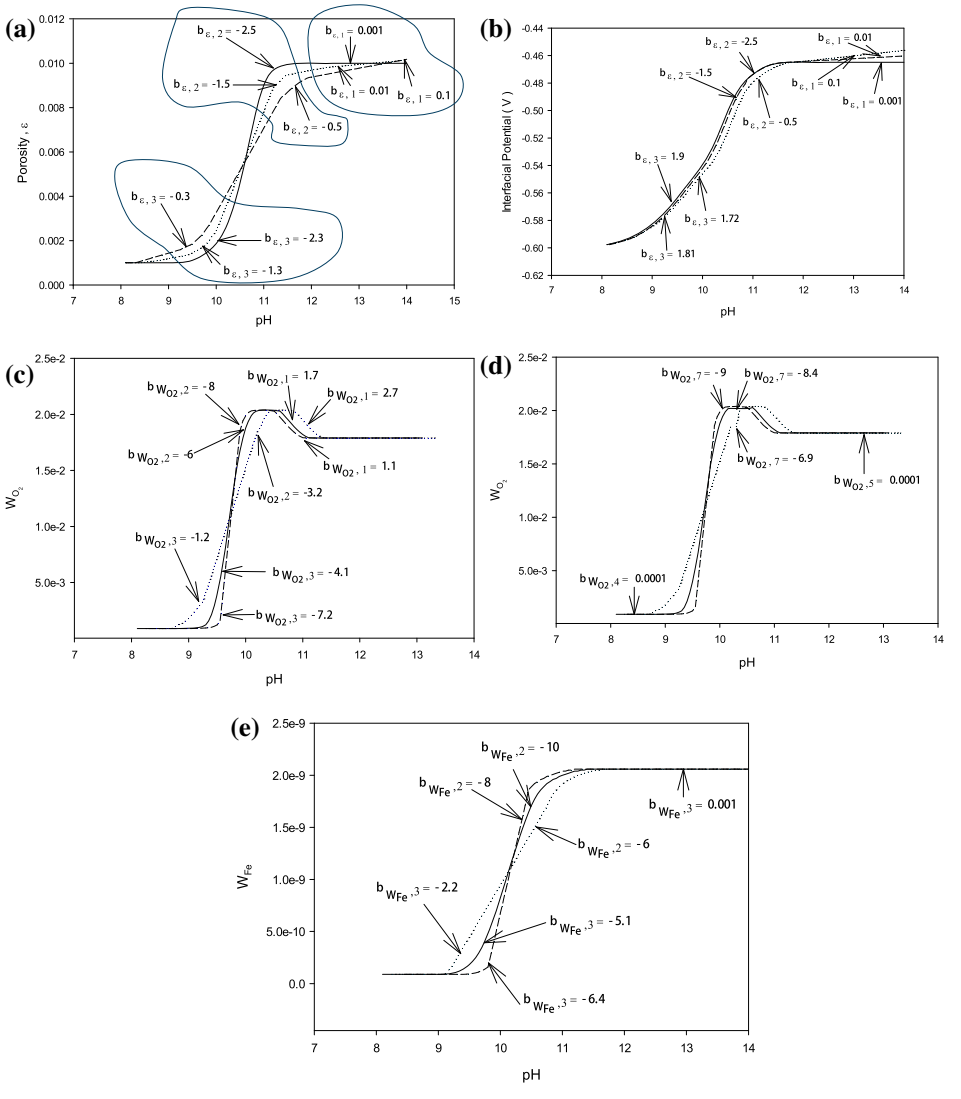

Figure 24. Sensitivity analysis of the fitting parameters for relationships: (a) ε–pH, (b) V–pH, (c) w_{O_2}–pH $(b_{w_{O_2},1} - b_{w_{O_2},3})$, (d) w_{O_2}–pH ($b_{w_{O_2},4}$ and $b_{w_{O_2},7}$), (e) w_{Fe}–pH.

dependency. The same situation also holds for the fitting parameter $b_{\varepsilon,1}$ in case of interfacial potential V–pH relationship shown in Figure 24(b) which shows the constant feature with only smaller $b_{\varepsilon,1}$ values. The fitting parameter $b_{\varepsilon,2}$ also termed as slope control parameter adjusts the porosity and potential slope. When $b_{\varepsilon,2}$ changes from –0.5 to –2.5, the slope of both the porosity and potential increases. Similarly the fitting parameter, $b_{\varepsilon,3}$ adjusts the initial slope for porosity and potential.

The effect of fitting parameters on polarisation parameters (w_{O_2} and w_{Fe}) is shown in Figure 24(c)–(e). The fitting parameters for w_{O_2} $(b_{W_{O_2},1} - b_{W_{O_2},7})$ in Figure 24(c) and (d) adjust the shape of w_{O_2} − pH relation. For instance, $b_{W_{O_2},2}$ adjusts the slope of the curve which becomes steeper from –0.5 to –2.5. This increase in the steepness of the curve attributes to the increase in potential and porosity front velocities; however, this parameter does not affect the delamination rate. Similarly, $b_{W_{O_2},1} - b_{W_{O_2},4}$ have similar effect on curve fitting as discussed for porosity and potential fitting parameters. Parameter $b_{W_{O_2},7}$ plays an important part in delamination rate as the smooth turn in the curve slope decides the pH value, for instance for parameter $b_{W_{O_2},7}$ from –6.9 to –9 the w_{O_2} value increases from $1.7e^{-2}$ to $2.1e^{-2}$. The parameter values and results for $b_{W_{O_2},7}$ are slight different from the results reported by Huang [17]. Parameter $b_{W_{O_2},7}$ directly affects polarisation parameter (w_{O_2}), further affecting oxygen reduction current density ($i_{O_2}^{coat}$) and therefore, affecting mass transfer limited mechanism. The delamination kinetics indicates the fitting parameters $b_{Fe,1}$ – $b_{Fe,4}$ in Figure 24(e) does not have any significant effect over the simulation results.

6. Application in prognostics – reliability modelling

6.1. *Initiation of metal-coating delamination*

The developed model in this research can be utilised in prognostics. Prognostics is the ability to predict accurately and precisely the RUL of a failing system.[37] In this research, the failing system is the metal-coating. The physical quantity to be predicted is the 'metal-coating bonding failure' due to delamination.

The ionic concentration c_S at the delaminated (porous) region reaches the threshold concentration c_S^{TH} at time t_n. Therefore, t_n corresponds to the instance at which the propagation of delaminated (porous) region along the metal-coating interface starts. The ionic threshold concentration c_S^{TH} along with time t_n defines the point of failure on a time graph and can be used to calculate RUL. The RUL is therefore defined as a projection (forecast) of the delamination rate (due to ionic concentration c_S) onto the time domain for a fixed value, referred to as the threshold concentration c_S^{TH}.

The PDE $f(z)$ (Equation (24)) for the ionic concentration is a probability density function (PDF) [38,39] over the time range of t_n to t_x. The PDE $f(z)$ has been solved and implemented in Section 4 using iterative algorithms (Proc. CTM, Proc. IPM and Proc. DCM). Where t_x is the time corresponding to the condition $c_S = 0$, at which the ionic concentration along the interface depletes. The cumulative density function (CDF) $F_{init}(t)$ is,

$$F_{init}(t) = \int_{t_n}^{t_x} f(z)dz \tag{36}$$

where $f = \overline{f_{c_s}}$. The term $\overline{f_{c_s}} = (f_{Fe}, f_{Na}, f_{OH})$ in Equation (28) is the symbolic representation of PDF in Equation (22). The PDF is used to analyse the concentration of ions (Fe^{2+}, Na^+ andOH^-) along the interface. The function $\overline{f_{c_s}}$ in Equation (28) can

again be written back in terms of ionic concentration representation, as in Equation (22), which gives the form as,

$$c_s(z,t) = c_{s(a)}(z) - c_s(z,g,t) \tag{37}$$

where $c_s(z,g,t)$ represent the ionic concentration inside the delaminated (porous) region at time t and distance x from the defect. The term g represents the coating thickness over the metal. The ionic concentration corresponding to the point of initiation of delamination $c_{s(a)}(z)$ is assumed to be always greater than $c_s(z,p_t,t)$.

6.2. Probability of metal-coating bonding failure

Equation (36) can be written in the form as,

$$f(z) = \frac{d}{dt} F_{\text{init}}(t) \tag{38}$$

The probability of metal-coating bonding failure $P(t)$ can be found by writing Equation (38) as,

$$P(t) = \frac{f(z)}{1 - F_{\text{init}}(t)} = \frac{f(t)}{N(t)} \tag{39}$$

where $f(z)$ in Equations (38) and (39) represent the probability of failure due to ionic concentration along the delaminated (porous) region. The term $N(t) = 1 - F_{\text{init}}(t)$ represents the probability of use without failure when $t \leq t_{\text{init}} < t_d$. $F_{\text{init}}(t)$is the cumulative density function and can be found using Equation (36)

7. Conclusions

A mathematical model is developed to simulate the delamination mechanism of coating due to the electrochemical reactions at metal-coating interface. The model is based on the observations from experiments. The mathematical model comprises three interdependent parallel processes, with each process having distinct novel equations. Each process models: cation formation, oxygen reduction and cation transport mechanism. The set of mathematical equations under each process are then solved and implemented by utilising efficient time-iterated algorithms, with separate algorithm for each process. The process algorithms communicate with each other using duplex channels carrying signals. Each signal represents a distinct delamination parameter. The processes comprise linear equations, PDEs and algebraic equations. The simulation results demonstrated the following facts regarding the cathodic delamination mechanism:

(1) Cations concentration and transport are the primary contributors to the debonding of metal-coating system. These parameters decide the delamination rate. The trends observed for the dependent variables are consistent with simulated and experimental trends reported in the literature.[10,16,40]
(2) The simulation results also confirm that polarisation parameters and interfacial porosity contribute towards the propagation of the front. The interfacial porosity accounts for the breakage of metal-coating bonding.
(3) The results for the propagation rates are sensitive to the rate constant for the ε (porosity)–pH relationship. This brings the contribution of interfacial porosity ε towards the propagation of the front into the light.

(4) The fitting parameters for ε–pH, V–pH, w_{O_2}–pH, w_{Fe}–pH relations seriously affect the simulation results. These fitting parameters are important in deciding the shapes of overall pH, porosity and polarisation parameter trends. Therefore, an accurate beforehand computation of these fitting parameters is required to get precise results.
(5) The developed model finds its implementation in prognostics in order to calculate the RUL of a metal-coating system.

Acknowledgement

This research is joint funded by Defence Science and Technology Laboratory (DSTL), Ministry of Defence (MoD) and Bournemouth University UK, the authors acknowledge their support and contributions.

Disclosure statement

No potential conflict of interest was reported by the authors.

Funding

This research is joint funded by Defence Science and Technology Laboratory (DSTL), Ministry of Defence (MoD) and Bournemouth University UK.

References

[1] Deflorian F, Rossi S. An EIS study of ion diffusion through organic coatings. Electrochim. Acta. 2006;51:1736–1744.
[2] Nazir MH, Khan ZA, Stokes K. A unified mathematical modelling and simulation for cathodic blistering mechanism incorporating diffusion and fracture mechanics concepts. J. Adhes. Sci. Technol. 2015;29:1200–1228. Available from: http://dx.doi.org/10.1080/01694243.2015.1022496
[3] Stratmann M, Leng A, Fürbeth W, Streckel H, Gehmecker H, Groβe-Brinkhaus K-H. The scanning Kelvin probe; a new technique for the in situ analysis of the delamination of organic coatings. Prog. Org. Coat. 1996;27:261–267.
[4] Ogle K, Morel S, Meddahi N. An electrochemical study of the delamination of polymer coatings on galvanized steel. Corros. Sci. 2005;47:2034–2052.
[5] Ogle K, Tomandl A, Meddahi N, Wolpers M. The alkaline stability of phosphate coatings I: ICP atomic emission spectroelectrochemistry. Corros. Sci. 2004;46:979–995.
[6] Tomandl A, Wolpers M, Ogle K. The alkaline stability of phosphate coatings II: in situ Raman spectroscopy. Corros. Sci. 2004;46:997–1011.
[7] Stratmann M, Feser R, Leng A. Corrosion protection by organic films. Electrochim. Acta. 1994;39:1207–1214.
[8] Grundmeier G, Reinartz C, Rohwerder M, Stratmann M. Corrosion properties of chemically modified metal surfaces. Electrochim. Acta. 1998;43:165–174.
[9] Leng A, Streckel H, Stratmann M. The delamination of polymeric coatings from steel. Part 1: calibration of the Kelvin probe and basic delamination mechanism. Corros. Sci. 1998;41:547–578.
[10] Leng A, Streckel H, Stratmann M. The delamination of polymeric coatings from steel. Part 2: first stage of delamination, effect of type and concentration of cations on delamination, chemical analysis of the interface. Corros. Sci. 1998;41:579–597.
[11] Leng A, Streckel H, Hofmann K, Stratmann M. The delamination of polymeric coatings from steel Part 3: effect of the oxygen partial pressure on the delamination reaction and current distribution at the metal/polymer interface. Corros. Sci. 1998;41:599–620.

[12] Fürbeth W, Stratmann M. The delamination of polymeric coatings from electrogalvanised steel – a mechanistic approach. Corros. Sci. 2001;43:207–227.
[13] Fürbeth W, Stratmann M. The delamination of polymeric coatings from electrogalvanized steel – a mechanistic approach. Corros. Sci. 2001;43:229–241.
[14] Fürbeth W, Stratmann M. The delamination of polymeric coatings from electrogalvanized steel – a mechanistic approach. Corros. Sci. 2001;43:243–254.
[15] Grundmeier G, Schmidt W, Stratmann M. Corrosion protection by organic coatings: electrochemical mechanism and novel methods of investigation. Electrochim. Acta. 2000;45:2515–2533.
[16] Allahar KN, Orazem ME, Ogle K. Mathematical model for cathodic delamination using a porosity–pH relationship. Corros. Sci. 2007;49:3638–3658.
[17] Huang M-W, Allely C, Ogle K, Orazem ME. A mathematical model for cathodic delamination of coated metal including a kinetic pH–porosity relationship. J. Electrochem. Soc. 2008;155:C279–C292.
[18] Nazir MH, Khan ZA, Stokes K. Optimisation of interface roughness and coating thickness to maximise coating-substrate adhesion – a failure prediction and reliability assessment modelling. J. Adhes. Sci. Technol. 2015;29:1415–1445. Available from: http://dx.doi.org/10.1080/01694243.2015.1026870
[19] Nazir MH, Khan Z, Stokes K. Modelling of metal-coating delamination incorporating variable environmental parameters. J. Adhes. Sci. Technol. 2015;29:392–423.
[20] Saeed A, Khan Z, Clark M, Nel M, Smith R. Non-destructive material characterisation and material loss evaluation in large historic military vehicles. Insight-Non-Destr. Test. Condition Monit. 2011;53:382–386.
[21] Saeed A, Khan ZA, Hadfield M, Davies S. Material characterization and real-time wear evaluation of pistons and cylinder liners of the Tiger 131 military tank. Tribol. Trans. 2013;56:637–644.
[22] Saeed A, Khan ZA, Montgomery E. Corrosion damage analysis and material characterization of Sherman and Centaur – the historic military tanks. Mater. Perform. Char. 2013;2:1–16.
[23] Nazir MH, Khan Z, Stokes K. The propagation and axisymmetric stability of circular, defect driven coating delamination under the influence of compression and diffusion induced stress. Eng. Fract. Mech., Elsevier [submitted].
[24] Khan ZA, Grover M, Nazir MH. The implications of wet and dry turning on the surface quality of EN8 steel. In: Transactions on Engineering Technologies, ed. Springer, 2015. p. 413–423.
[25] Nazir MH, Khan ZA, Stokes K. Maximising the interfacial toughness of thin coatings and substrate through optimisation of defined parameters, Int. J. Comput. Methods Exp. Meas. (WIT Press), (in press).
[26] Khan ZA, Pashaei P, Bajwa RS, Nazir MH, Camak M, Fabrication and characterisation of electrodeposited and magnetron sputtered thin films, Int. J. Comput. Methods Exp. Meas. (WIT Press), (in press).
[27] Belina F, Hogrefe D. The CCITT-specification and description language SDL. Comput. Networks ISDN Syst. 1989;16:311–341.
[28] Swan S. An introduction to system level modeling in System C 2.0. Cadence Design Systems, Inc., draft report; 2001.
[29] Sarikaya O. Effect of some parameters on microstructure and hardness of alumina coatings prepared by the air plasma spraying process. Surf. Coat. Technol. 2005;190:388–393.
[30] Steinbuch M, Audran R. The isolation of IgG from mammalian sera with the aid of caprylic acid. Arch. Biochem. Biophys. 1969;134:279–284.
[31] Grahame DC. Diffuse double layer theory for electrolytes of unsymmetrical valence types. J. Chem. Phys. 1953;21:1054–1060.
[32] Laidler KJ. The development of the Arrhenius equation. J. Chem. Educ. 1984;61:494–498.
[33] Newman J. Electrochemical engineering. Englewood Cliffs, NJ: Prentice-Hall; 1991.
[34] Grimmes S, Martinsen Ø. Electrolytics. In: Bioimpedance and bioelectricity basics; San Diego, CA: Academic Press; 2000. p. 3–50. ISBN: 978-0-12-303260-7.
[35] Mejlbro L. The complete solution of Fick's second law of diffusion with time-dependent diffusion coefficient and surface concentration. Lund: Technical University of Denmark; 1996.

[36] Manzanares J A and Kontturi K Diffusion and migration. In: Encyclopedia of electrochemistry; Vol. 2, Weinheim: Wiley-VCH; 2003. p. 81–145.
[37] Vachtsevanos G, Lewis F, Roemer M, Hess A, Wu B. Intelligent fault diagnosis and prognosis for engineering systems; 2006. 454 p Isbn, vol. 13, p. 978-0.
[38] Parzen E. On estimation of a probability density function and mode. Ann. Math. Stat. 1962;33:1065–1076.
[39] Hartzell AL, da Silva MG, and Shea HR. Lifetime prediction. In: MEMS reliability. New York: Springer; 2011. p. 9–42.
[40] Melchers RE, Jeffrey R. Early corrosion of mild steel in seawater. Corros. Sci. 2005;47:1678–1693.